Cell

Origin and Function of Stress-Induced IL-6 in Murine Models

Graphical Abstract

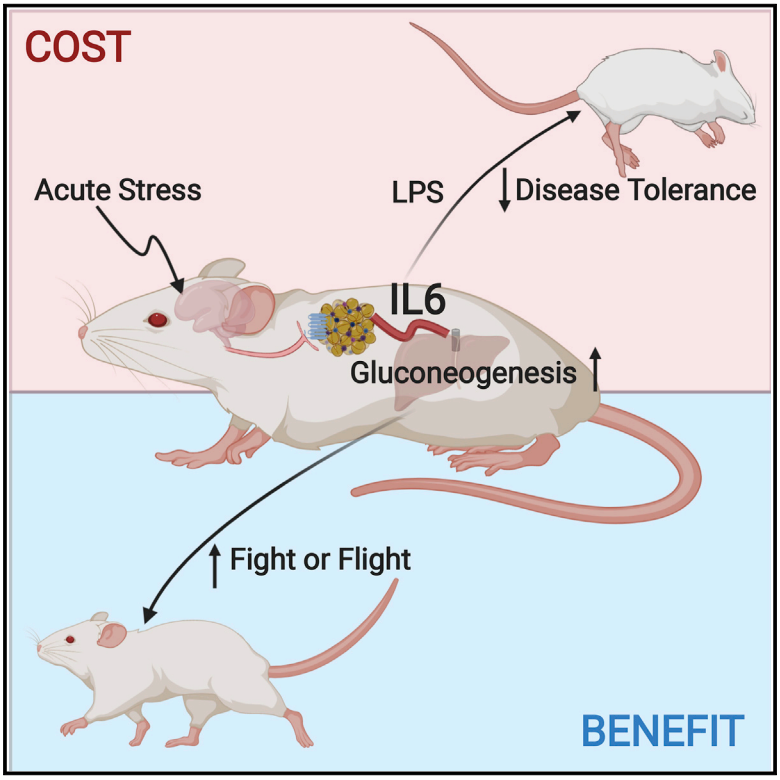

Authors

Hua Qing, Reina Desrouleaux, Kavita Israni-Winger, ..., Marina R. Picciotto, Rachel J. Perry, Andrew Wang

Correspondence

andrew.wang@yale.edu

In Brief

During acute psychological stress, brown adipocytes initiate a chain of events mediated by adrenergic signaling and IL-6 release that metabolically fuels "fight or flight" adaptive responses but at the same time comes at an inflammatory cost.

Highlights

- IL-6 is the dominant endocrine cytokine induced by acute stress in mice
- Stress-inducible IL-6 is produced in brown adipocytes via ADRB3 signaling
- IL-6 is required for stress hyperglycemia and adaptive "fight or flight" responses
- Stress-induced IL-6 decreases tolerance to a subsequent inflammatory challenge

Qing et al., 2020, Cell *182*, 1–16
July 23, 2020
https://doi.org/10.1016/j.cell.2020.05.054

Please cite this article in press as: Qing et al., Origin and Function of Stress-Induced IL-6 in Murine Models, Cell (2020), https://doi.org/10.1016/j.cell.2020.05.054

Cell

CellPress

Article

Origin and Function of Stress-Induced IL-6 in Murine Models

Hua Qing,[1,2,7] Reina Desrouleaux,[1,2,6,7] Kavita Israni-Winger,[2] Yann S. Mineur,[4] Nia Fogelman,[3] Cuiling Zhang,[1,2] Saleh Rashed,[2] Noah W. Palm,[2] Rajita Sinha,[3] Marina R. Picciotto,[4] Rachel J. Perry,[5] and Andrew Wang[1,2,8,*]

[1]Department of Medicine (Rheumatology, Allergy & Immunology), Yale University School of Medicine, New Haven, CT, USA
[2]Department of Immunobiology, Yale University School of Medicine, New Haven, CT, USA
[3]Yale Stress Center and Departments of Psychiatry and Neuroscience, Yale School of Medicine, New Haven, CT, USA
[4]Department of Psychiatry, Yale Interdepartmental Neuroscience Program, Yale University, New Haven, CT, USA
[5]Departments of Medicine (Endocrinology) and Cellular and Molecular Physiology, Yale University, New Haven, CT, USA
[6]Present address: Case Western Reserve University School of Medicine, Cleveland, OH, USA
[7]These authors contributed equally
[8]Lead Contact
*Correspondence: andrew.wang@yale.edu
https://doi.org/10.1016/j.cell.2020.05.054

SUMMARY

Acute psychological stress has long been known to decrease host fitness to inflammation in a wide variety of diseases, but how this occurs is incompletely understood. Using mouse models, we show that interleukin-6 (IL-6) is the dominant cytokine inducible upon acute stress alone. Stress-inducible IL-6 is produced from brown adipocytes in a beta-3-adrenergic-receptor-dependent fashion. During stress, endocrine IL-6 is the required instructive signal for mediating hyperglycemia through hepatic gluconeogenesis, which is necessary for anticipating and fueling "fight or flight" responses. This adaptation comes at the cost of enhancing mortality to a subsequent inflammatory challenge. These findings provide a mechanistic understanding of the ontogeny and adaptive purpose of IL-6 as a bona fide stress hormone coordinating systemic immunometabolic reprogramming. This brain-brown fat-liver axis might provide new insights into brown adipose tissue as a stress-responsive endocrine organ and mechanistic insight into targeting this axis in the treatment of inflammatory and neuropsychiatric diseases.

INTRODUCTION

Acute life stressors have been observed to decompensate a wide range of inflammatory diseases since antiquity (Hippocrates, 1849; Liu et al., 2017). Most chronic sterile inflammatory diseases are known to "flare" after acute stress, contributing significantly to morbidity and mortality. Indeed, psychosocial stress worsens most inflammatory diseases, including allergic diseases, autoimmune diseases, and cancers (Batty et al., 2017; Liu et al., 2002; Mohr et al., 2004; Roussou et al., 2013). In human studies, stress induces measurable changes in biology, such as in the magnitude of inflammatory cytokines and in functional changes within relevant end-organs, such as in pulmonary function in the case of allergic inflammation (Liu et al., 2002). Concordantly, several randomized controlled trials targeting stress management have largely lead to improvement in the morbidity of inflammatory diseases (Black and Slavich, 2016; Pbert et al., 2012; Simpson et al., 2014). However, the well-studied mediators of stress physiology, glucocorticoids, and catecholamines, are primarily thought to be immunosuppressive (Russell and Lightman, 2019) and used therapeutically for this purpose, creating a paradox that many have tried to resolve for over 30 years (Frank et al., 2013; Munck et al., 1984). How does psychological stress, which leads to the production of immunosuppressive mediators such as cortisol and catecholamines, decrease host fitness to inflammation?

Studies dating back to 1990 have shown that psychological stress increases circulating levels of interleukin-6 (IL-6) in humans and laboratory animals (Cheng et al., 2015; LeMay et al., 1990; Maes et al., 1998). The role that IL-6 plays in the acute stress response, also referred to as the "fight or flight" response, is unclear. The idea that stress itself induces endocrine mediators like IL-6, which is traditionally associated with inflammation, has since been supported by the detection of increased circulating cytokines in depression and anxiety (Felger and Lotrich, 2013; Khandaker et al., 2014) and by the association of IL-6 polymorphisms in individuals with depression (Zhang et al., 2016). Moreover, there is a robust relationship between depression and anxiety and poor outcomes in inflammatory diseases (Eisner et al., 2005; Satin et al., 2009). This body of research has led to clinical trials assessing the efficacy of an antagonizing monoclonal antibody targeting IL-6 receptor subunit alpha (IL-6Ra), tocilizumab—used in rheumatoid arthritis and vasculitis—in depression (Kappelmann et al., 2018), despite little

Please cite this article in press as: Qing et al., Origin and Function of Stress-Induced IL-6 in Murine Models, Cell (2020), https://doi.org/10.1016/j.cell.2020.05.054

understanding of how and why stress induces IL-6. The possibility that stress-inducible cytokines, as opposed to glucocorticoids or catecholamines, underlie how stress leads to poorer outcomes in inflammatory diseases has not been explored in depth.

Here, we report that commonly utilized models of acute stress in mice induce endocrine IL-6. Stress-induced IL-6 requires consciousness and beta-3-adrenergic-receptor signaling in brown adipocytes. IL-6 is required for stress hyperglycemia, a metabolic adaptation that enables the "fight or flight" response, via hepatic gluconeogenesis. The cost of stress-induced IL-6 is that it decreases host fitness to a subsequent inflammatory challenge. Our studies therefore mechanistically uncover the origin and adaptive function of IL-6 in acute stress and its cost in the setting of inflammation in mice.

RESULTS

Acute stress induces endocrine IL-6

We found that standard laboratory models of acute stress—including tube restraint, cage switching, and social isolation—induced high levels of circulating IL-6 (Figure 1A), consistent with previous studies demonstrating that stress alone induced IL-6 (Cheng et al., 2015; LeMay et al., 1990; Maes et al., 1998). Unexpectedly, we found that a single, conscious, retro-orbital bleed induced IL-6 (Figure 1A). To more comprehensively survey other stress-inducible immune mediators, we screened 32 inflammatory cytokines and chemokines in the circulation of stressed mice and identified a set of cytokines inducible by stress alone; IL-6 was the most greatly induced cytokine and common to two different stress models (Figure 1B). We did not detect corresponding increases in the soluble IL-6 receptor (Figure S1A) (Khokha et al., 2013). The absolute level of IL-6 we detected fell in the middle range of reported levels (50 pg/mL to 200 ng/mL) in inflammatory contexts and above reported ranges post-exercise and in diet-induced obesity (30–100 pg/mL) (Chowdhury et al., 2020; Gao et al., 2014; Greenhill et al., 2011; Masuda et al., 2013; Osuchowski et al., 2006; Remick et al., 2005; Vida et al., 2015; Wang et al., 2017; Yan et al., 2015). We also confirmed that acute, stress-increased IL-6 was independent of handlers (as indicated Figure 1A–C).

To exclude circadian oscillations leading to fluctuations in IL-6, we measured circulating IL-6 over time by retro-orbital bleeding and observed that repeated bleeding of the same animals sustained high IL-6 levels. When individual cages of unmanipulated, entrained animals were bled at the corresponding Zeitgeber times (five mice per ZT time, bled only once at that ZT time), no such sustained increase in IL-6 was noted, demonstrating that conscious bleeding itself increased circulating IL-6 and that repeated bleeding sustained high IL-6 levels (Figure 1C). Thus, in order to gain insight into the kinetics of IL-6 after an acute stress, we subjected several groups of mice to a single retro-orbital bleed, and then sampled individual groups at different time points after the bleed. Circulatory cortisol and noradrenaline were increased within 15 min, peaked at 2 h after acute stress, and returned to baseline by 4 h; however, IL-6, which was significantly increased in blood by 2 h, peaked at 4 h, and was even detectable above baseline 18 h after acute stress (Figure 1D). The unique kinetics of stress-induced endocrine IL-6 suggested that it may be mediating more sustained aspects of stress physiology.

Because the adrenal gland is thought to be the major mediator of the acute stress response, and previous reports have described adrenally derived IL-6 (Päth et al., 2000), we asked if the adrenal gland was required for stress-induced IL-6. We found that adrenalectomized mice had significantly higher levels of IL-6 after stress, suggesting that the adrenal gland negatively regulated IL-6 (Figure S1B). To address previous reports of cross-talk between IL-6 and adrenal hormones (Bethin et al., 2000; Päth et al., 2000), we utilized an antagonistic anti-IL-6Ra antibody and found that inhibition of IL-6 signaling did not change circulating levels of corticosterone or noradrenaline after acute stress (Figures S1C and S1D). This model avoids the confounding developmental defects observed in constitutive IL-6 knockout animals (Wallenius et al., 2002).

We then validated previous observations that circulating IL-6 levels were increased in stressed humans (Felger and Lotrich, 2013; Khandaker et al., 2014). We acquired a community sample of individuals that were carefully assessed for high and low stress by using a structured cumulative stress and adversity interview that assessed recent and past life events (Cumulative Adversity Interview) (Ansell et al., 2012; Seo et al., 2014; Turner and Lloyd, 1995). The high and low groups were group matched by age, gender, education, and body mass index (Figure S1E). We found significant overall increased IL-6 levels in the high (74 pg/mL, SE: 35) versus low (3.9 pg/mL, SE: 2.78) stress groups ($t = 2.15$, $p < 0.05$) (Figure S1E). The absolute circulating level of stress-associated IL-6 in humans was a hundred times lower in mice, reflecting inter-species variation and/or acuity, heterogeneity, and magnitude of stressors. Taken together, these data indicate that IL-6 is an endocrine hormone inducible by acute stress alone, with different kinetics than the canonical stress hormones, corticosterone and noradrenaline.

Stress-inducible IL-6 is produced by brown adipocytes

To understand the ontogeny of stress-induced IL-6, we first ensured that IL-6 was not induced by retro-orbital bleeding as a result of bacterial translocation from the skin or gastrointestinal tract (Kelly et al., 2015). Consistent with our observations that other acute-phase cytokines were not induced after stress, stress-induced IL-6 was present in both gnotobiotic animals and animals deficient in key signaling pathways necessary for detecting bacteria (Figure 2A). Previous reports had suggested that hyperglycemia itself, a characteristic feature of the acute stress response (Esposito et al., 2002), was sufficient to induce IL-6. To test this, we performed an oral glucose tolerance test 4 h post retro-orbital bleeding and found that both glucose and water induced IL-6, suggesting that the acute stress of gavaging and bleeding, but not hyperglycemia, was responsible for IL-6 induction (Figures S1F and S1G). We also wanted to exclude the possibility that local damage to the retro-orbital plexus was inducing regional endothelial or immune release of IL-6, and so we sampled the contralateral orbital plexus and did not observe differences between traumatized and untraumatized eyes, suggesting that the contribution of systemic IL-6 was not significantly affected by local damage (Figure S1H).

Please cite this article in press as: Qing et al., Origin and Function of Stress-Induced IL-6 in Murine Models, Cell (2020), https://doi.org/10.1016/j.cell.2020.05.054

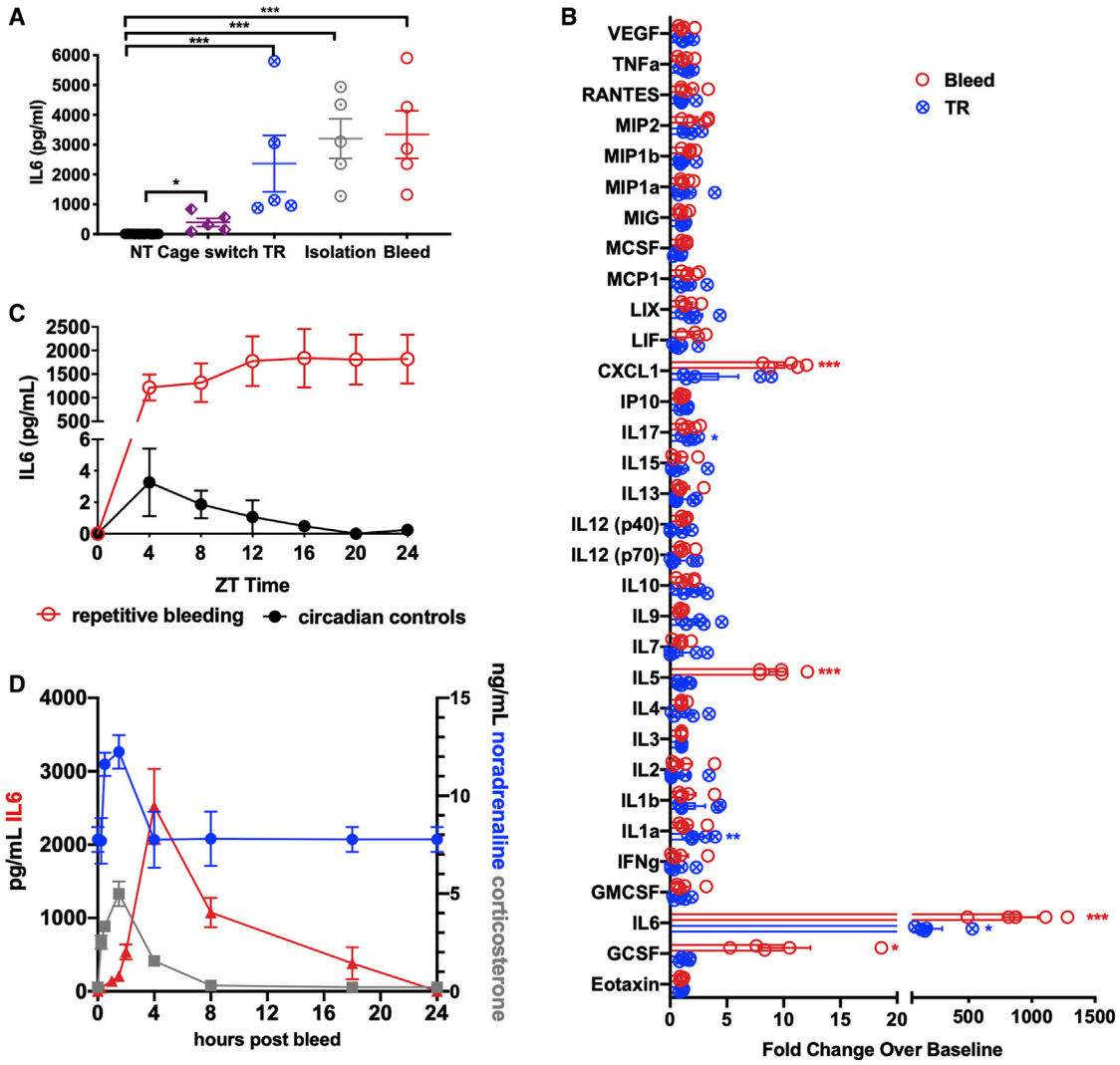

Figure 1. Acute stress induces endocrine IL-6

(A) Plasma IL-6 levels in mice after exposure to one of the indicated stress challenges (n = 5 per group, representative of 2 experiments). These experiments were performed by H.Q. NT, no treatment; TR, tube restraint.

(B) Fold change of the indicated inflammatory cytokines and chemokines 4 h after a single retro-orbital bleed or tube restraint (TR). Results are presented as the ratio of cytokine or chemokine levels from stressed subjects compared with no stress controls (n = 5 per group). Experiments were performed by R.D.

(C) Plasma IL-6 levels after repetitive bleeding. Repetitive bleeding was applied to the same mice (n = 5) every 4 h, while circadian controls were non-stressed mice bled once at the indicated ZT times (n = 5 for each time point). Experiments were performed by A.W.

(D) Plasma levels of noradrenaline, corticosterone, and IL-6 post bleeding at indicated time point (n = 5 per time point, representative of 2 experiments). Data are represented as mean ± SEM. *p < 0.05, **p < 0.01, ***p < 0.001, ****p < 0.0001.

See also Figures S1 and S7.

IL-6 is produced by many cell types, including hematopoietic cells, myocytes, endothelial cells, and adipocytes (Hunter and Jones, 2015). To identify the origin of IL-6, we first performed mixed bone marrow chimera studies by using IL-6-deficient animals and found that stress-induced IL-6 was not produced by radiosensitive cells (Figure 2B). Given the kinetics of plasma IL-6 after acute stress, we reasoned that IL-6 would be transcriptionally regulated. Thus, we screened multiple tissues for *Il6* induction using both the bleeding and tube restraint models. We found that *Il6* was robustly induced in the brown adipose tissue (BAT) (Figure 2C) and confirmed protein expression by immunohistochemistry (Figure 2D). We did not detect increased muscle *Il6*, which was consistent with the observation that mice did not significantly increase physical activity after an acute stressor (Figure S2B). To test if BAT was the sole source of stress-induced IL-6, we surgically excised the BAT, which ablated the IL-6 response to bleeding stress (Figure 2E).

Because BAT is a complex collection of cells including radioresistant immune cells (Wolf et al., 2017), we first asked if stress-

Please cite this article in press as: Qing et al., Origin and Function of Stress-Induced IL-6 in Murine Models, Cell (2020), https://doi.org/10.1016/j.cell.2020.05.054

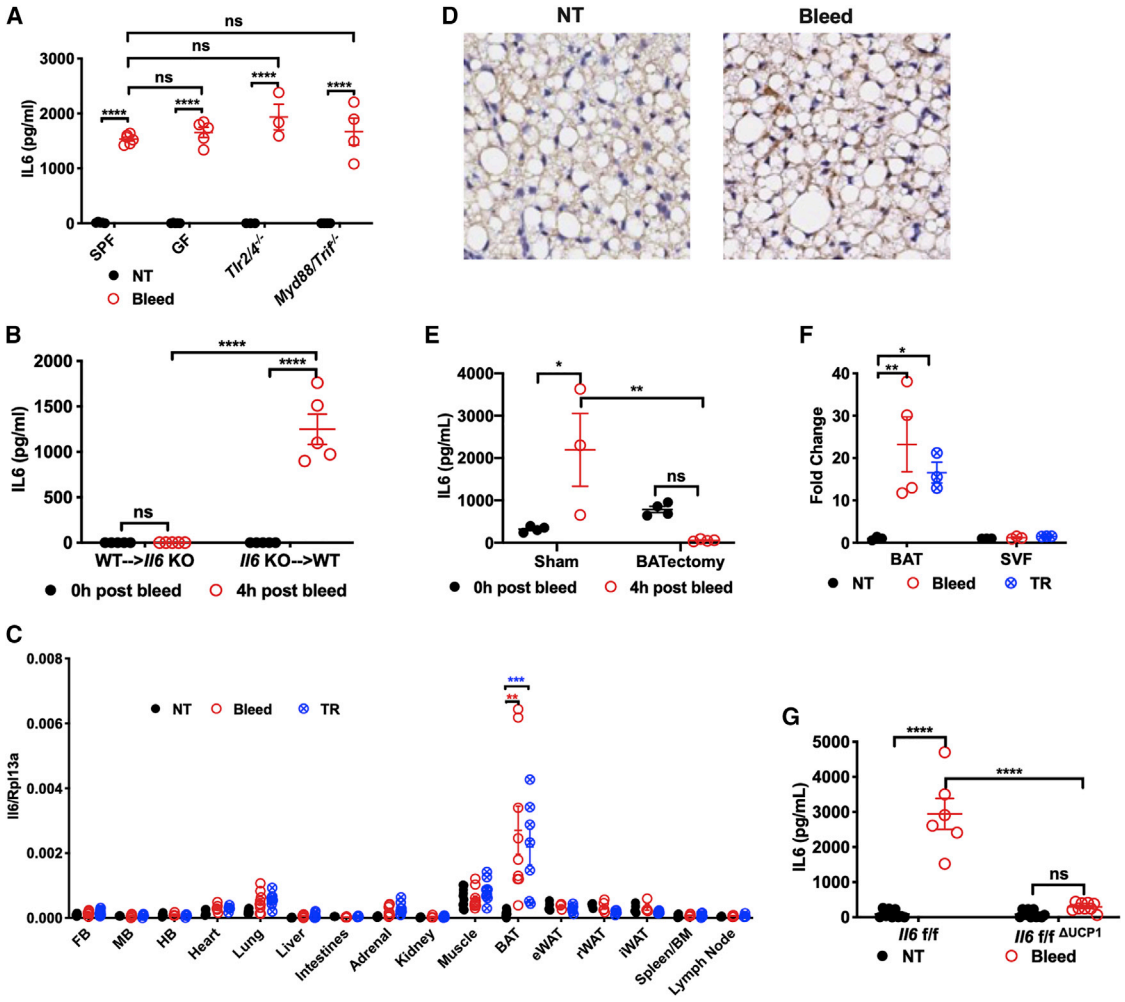

Figure 2. Stress-inducible IL-6 is produced by brown adipocytes

(A) Plasma levels of IL-6 after retro-orbital bleeding from conventionally housed mice (SPF), germ free mice (GF), or mice deficient in key signaling pathways necessary for pathogen detection and response (n = 8 for SPF, n = 5for GF, n = 3 for *Tlr2/4*$^{-/-}$, n = 4 for *Myd88/Trif*$^{-/-}$).

(B) Plasma level of IL-6 from chimeric mice exposed to bleeding. WT → *Il6* KO: *Il6* knockout (KO) mice transplanted with bone marrow (BM) cells from wild-type (WT) mice; *Il6* KO → WT: WT mice transplanted with BM cells from *Il6* KO mice (n = 5 per group).

(C) Transcriptional analysis of *Il6* in tissues from stressed and control mice (n = 5 per group, representative of 2 experiments). Abbreviations are as follows: FB, forebrain; MB, midbrain; HB, hindbrain; BAT, brown adipose tissue; eWAT, epididymal white adipose tissue; rWAT, retroperitoneal white adipose tissue; iWAT, inguinal white adipose tissue; NT, no treatment; TR, tube restraint.

(D) Representative images of immunohistochemical staining for IL-6 in brown adipose tissue harvested from bled mice or from controls (NT). IL-6-positive staining is brown.

(E) Plasma level of IL-6 post bleeding from mice with surgical removal of brown adipose tissue (BATectomy) or sham surgery controls (sham) (n = 3 for sham, n = 4 for BATectomy).

(F) Transcriptional analysis of *Il6* in stromal vascular fraction (SVF) of brown adipose tissue (BAT) from stressed mice (n = 3 for NT, n = 4 for Bleed or TR group, representative of 2 experiments). Results are presented as fold increase in relation to non-stressed controls (NT). TR, tube restraint.

(G) Plasma level of IL-6 after bleeding from mice with *Il6* genetically deleted in brown adipocytes (*Il6*f/f$^{\Delta UCP1}$) compared with littermate controls (*Il6*f/f). NT, no treatment. Data are represented as mean ± SEM. *p < 0.05, **p < 0.01, ***p < 0.001, ****p < 0.0001.

See also Figure S1.

induced *Il6* would be present in the stromal vascular fraction (SVF), which includes all cells except adipocytes. The purity of our SVF isolation was verified by the absence of *Ucp1* and beta-3 adrenergic receptor (*Adrb3*) expression (Figures S1I and S1J). *Il6* transcriptional induction was not observed in the SVF fraction from either bled or restrained animals, implying that stress-induced IL-6 was derived from brown adipocytes (Figure 2F). Thus, we generated an animal in which *Il6* could be inducibly deleted in brown adipocytes by using *Ucp1* promoter-driven Cre under the control of estrogen receptor (*Il6*f/f$^{\Delta UCP1}$) and detected a significant attenuation of IL-6 after acute stress in these animals (Figure 2G). Collectively, our data demonstrate that brown adipocytes are the source of stress-induced IL-6.

Please cite this article in press as: Qing et al., Origin and Function of Stress-Induced IL-6 in Murine Models, Cell (2020), https://doi.org/10.1016/j.cell.2020.05.054

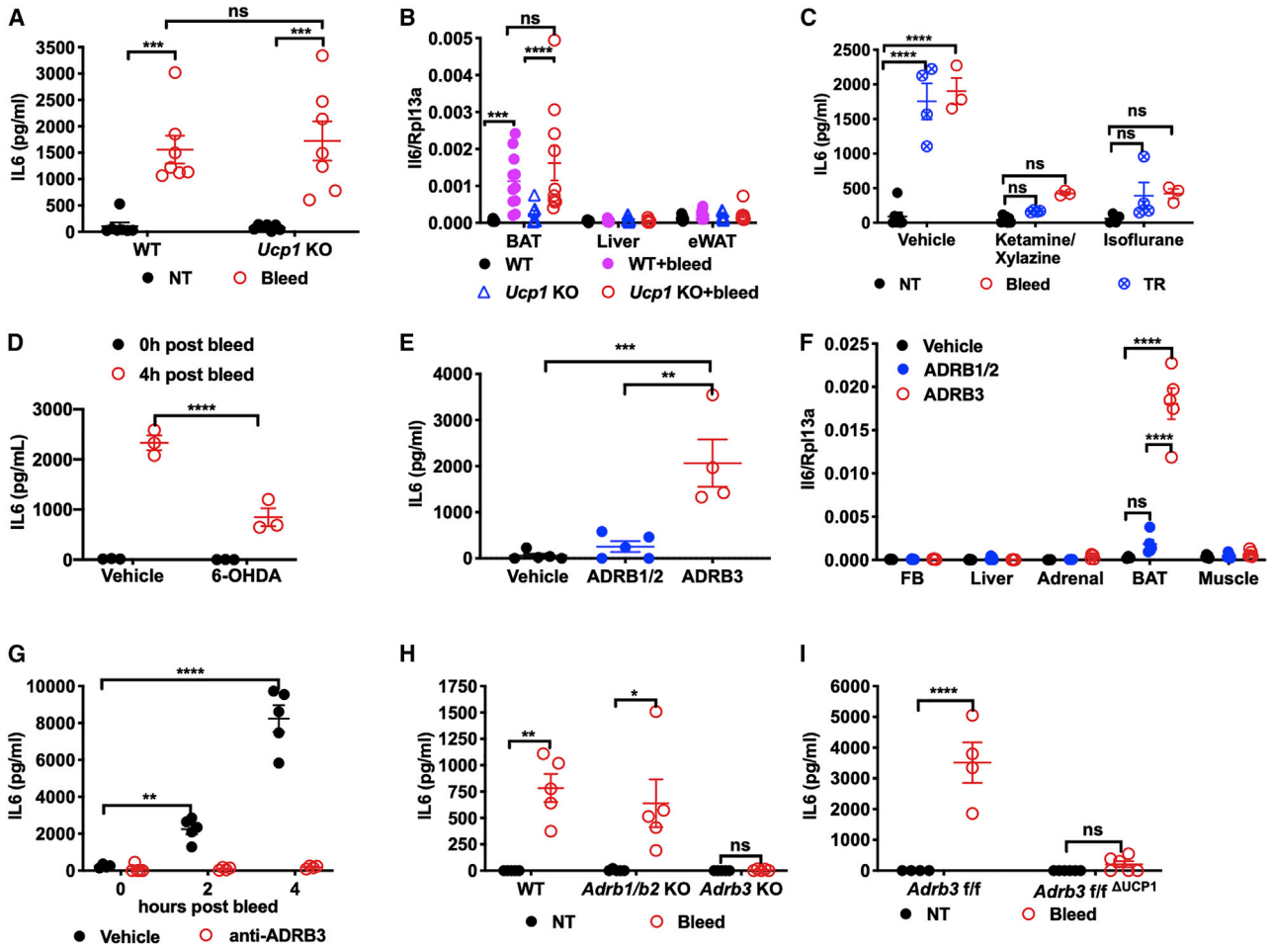

Figure 3. ADRB3 mediates brown adipocyte-derived IL-6 in response to acute stress

(A and B) Circulating IL-6 levels (n = 7 per group) (A) and mRNA expression of *Il6* post bleeding (B) in *Ucp1* KO or WT mice (n = 7 for WT, n = 11 for WT + bleed, n = 7 for *Ucp1* KO, n = 10 for *Ucp1* KO + bleed). NT, no treatment; BAT, brown adipose tissue; eWAT, epididymal white adipose tissue.

(C) Plasma IL-6 levels in mice bled or restrained after anesthesia induced by ketamine/xylazine or isoflurane (n = 3 for Bleed, n = 4 for TR, representative of 2 experiments). NT, no treatment; TR, tube restraint.

(D) Circulating IL-6 post bleeding from mice with chemical denervation of brown adipose tissue via 6-hydroxydopamine (6-OHDA) administration (n = 3 per group).

(E and F) Circulating IL-6 levels (E) and mRNA expression of *Il6* (F) 2 h post injection of beta-adrenergic receptor agonists (n = 5 per group). Abbreviations are as follows: ADRB1/ADRB2: isoproterenol, ADRB1 and ADRB2 agonist. ADRB3: CL316,243, ADRB3 agonist. FB, forebrain; Adrenal, adrenal gland; BAT, brown adipose tissue.

(G) Plasma level of IL-6 after bleeding at indicated time points from mice pre-treated with the ADRB3 antagonist SR59203A (n = 5 per group).

(H) Plasma level of IL-6 after bleeding in *Adrb1/2* KO or *Adrb3* KO mice (n = 5 per group). NT, no treatment.

(I) Plasma level of IL-6 after bleeding from mice with conditional *Ucp1*-mediated *Adrb3* deletion (*Adrb3*f/f$^{\Delta UCP1}$) or littermate controls (*Adrb3*f/f) (n = 5 per group). NT, no treatment. Data are represented as mean ± SEM. *p < 0.05, **p < 0.01, ***p < 0.001, ****p < 0.0001.

See also Figures S1 and S7.

ADRB3 mediates brown-adipocyte-derived IL-6 in response to acute stress independently of thermoregulation

Because BAT is critical for non-shivering thermogenesis in cold and psychological stress (Kataoka et al., 2014), we assessed the effect of ambient temperature on stress-induced IL-6. We subjected animals placed in standard cold acclimation (4°C), standard (22°C), and thermoneutral (32°C) conditions to bleeding stress, and did not note any effect on IL-6 induction (Figure S1K). To test whether the key mediator of non-shivering thermogenesis, UCP1, was required for IL-6, we tested the IL-6 response in *Ucp1*-deficient animals. Consistent with a function independent from thermoregulation, we did not note differences in either endocrine IL-6 levels or BAT transcriptional upregulation of *Il6* (Figures 3A and 3B). We also did not note any temperature differences after bleeding stress in the presence of IL-6Ra-blocking antibody compared with the isotype control (Figure S1L). Transcriptional analyses of BAT after acute stress did not demonstrate induction of *Ucp1* or other classic cold-responsive genes (Figure S1M). Interestingly, mRNA transcript for *Il5*, which was detected as a stress-induced cytokine after bleeding (Figure 1B), was also produced in the BAT. This finding is reminiscent of the

Please cite this article in press as: Qing et al., Origin and Function of Stress-Induced IL-6 in Murine Models, Cell (2020), https://doi.org/10.1016/j.cell.2020.05.054

reported role of IL-5 in BAT adaptation to prolonged cold exposure (Lee et al., 2015; Qiu et al., 2014).

We reasoned that consciousness would be required for IL-6 response to acute stress. Thus, we anesthetized animals with either ketamine/xylazine or isoflurane, after which we subjected them to tube restraint or retro-orbital bleeding and found that anesthesia abrogated stress-induced IL-6 (Figure 3C). Because sympathetic outflow to BAT is well-described in settings of acute exposure to cold (Kawate et al., 1994; Nguyen et al., 2017) and psychological stress (Kataoka et al., 2014), where projections originate from the rostral medullary raphe region and dorsomedial hypothalamus, we hypothesized that IL-6 was induced via beta-adrenergic signaling. To test if sympathetic neurons were required for stress-induced IL-6, we utilized 6-hydroxydopamine (6-OHDA) at doses that achieve significant BAT sympathectomy without significant effects on the CNS (Depocas et al., 1984). After 6-OHDA treatment, we found that stress-inducible IL-6 was significantly attenuated, confirming that sympathetic outflow was required (Figure 3D). Because all three beta-adrenergic receptors are present in BAT (Figures S1J, S1N, and S1O), we asked which of these played a role in mediating stress-induced IL-6. We thus challenged animals with ADRB agonists and found that the ADRB3 agonist CL316,243, but not the ADRB1/2 agonist isoproterenol, was sufficient to induce IL-6 (Figures 3E and 3F), consistent with previous reports (Kosteli et al., 2010; Zhang et al., 2014). Concordantly, pre-treatment with the pharmacologic inhibitor of ADRB3, but not ADRB1/2 (Figures 3G and S1P) or genetic deletion of *Adrb3* (Figure 3H), abrogated stress-induced IL-6. These experiments demonstrate that ADRB3 is necessary and sufficient for acute-stress-induced IL-6. Because many cell types express *Adrb3*, we generated animals in which *Adrb3* could be inducibly deleted from brown adipocytes (*Adrb3*f/f$^{\Delta UCP1}$) and verified that tamoxifen induction efficiently deleted *Adrb3* (Figure S1Q). As expected, and consistent with *Il6*f/f$^{\Delta UCP1}$ animals (Figure 2G), stress-inducible IL-6 was significantly attenuated in *Adrb3*f/f$^{\Delta UCP1}$ mice (Figure 3I). These data are consistent with a UCP1-independent ADRB3-dependent endocrine function of brown adipocytes and suggest that BAT may function as an endocrine organ sensitive to adrenergic outflow triggered by acute stress.

IL-6 is necessary for maintaining hyperglycemia after acute stress

Given the large induction of IL-6 by stress alone, we hypothesized that IL-6 was coordinating stress physiology. Classical "fight or flight" physiology includes autonomic outflow and metabolic reprogramming toward catabolic metabolism, which is thought to fuel the increased energy demand anticipated in threatening situations (Russell and Lightman, 2019). We did not detect significant changes in the quantity of canonical stress hormones (Figures S1C and S1D) or stress-induced heart rate or hypertension (Figure S2A) after acute stress in the absence of IL-6 function, suggesting that autonomic output was not significantly impacted by IL-6. In contrast, using indirect calorimetry, we did detect significant differences in the overall energy expenditure of stressed animals in which IL-6 signaling was antagonized (Figure 4A) despite no significant changes in total activity of animals in either group (Figure S2B). We thus hypothesized that organismal metabolic re-programming was likely a key function of stress-induced IL-6, consistent with the numerous studies that have reported a role for IL-6 in affecting organismal metabolism in various contexts (Covarrubias and Horng, 2014; Mauer et al., 2014; Pedersen and Febbraio, 2007; Scheller et al., 2011; Timper et al., 2017).

We thus examined metabolic changes induced by acute stress at the peak of endocrine IL-6 levels. We found that stress-induced hyperglycemia was durable at 4 h after acute stress in an IL-6Ra-dependent fashion (Figure 4B). A single bolus of stress-dosed IL-6 was also sufficient to recapitulate the effects of acute stress (Figure S2C), indicating that IL-6 was both necessary and sufficient to induce stress-hyperglycemia at this time point. Hyperglycemia is caused by impaired clearance (insulin resistance) and/or excess glucose production from glycogenolysis or gluconeogenesis. To determine which of these processes was causing hyperglycemia, we tested organismal insulin resistance with a glucose tolerance test (GTT) and did not detect significant differences between stressed and unstressed animals (Figure S2D). Likewise, we did not detect differences in GTT in mice challenged with a single bolus of stress-dosed IL-6 (Figure S2E) nor did we detect changes in plasma insulin at peak glycemia after IL-6 challenge (Figure S2F), suggesting the absence of an effect of IL-6 on insulin-dependent glucose uptake. However, when we performed insulin tolerance tests (ITT), we observed that acute stress alleviated insulin-induced hypoglycemia at later time points (Figure S2G), suggesting that stress-induced IL-6 might potentiate endogenous glucose production. Consistent with this idea, a single dose of recombinant IL-6 was also sufficient to recapitulate the effects of acute stress on maintaining higher levels of glucose at late time points during ITT (Figure S2H), and IL-6Ra blockade in stressed animals attenuated the ability of mice to maintain normoglycemia after insulin challenge (Figure S2I). We tested the contribution of glycogenolysis to stress hyperglycemia by examining glycogen content in liver, kidney, and skeletal muscle after stress but did not detect significant differences (Figure S2J). We thus hypothesized that IL-6 was inducing gluconeogenesis during stress.

Gluconeogenesis is typically engaged in hypoglycemic or net negative energy balance states, with the exception of forced intensive exercise, where muscle-derived IL-6 has been shown to induce gluconeogenesis (Banzet et al., 2009; Febbraio et al., 2004). To test if gluconeogenesis was impaired in an IL-6-dependent fashion, we measured endogenous glucose production after acute stress and found that it was significantly decreased in the absence of IL-6 signaling (Figure 4C). This finding was supported by pyruvate tolerance tests (PTT) in stressed animals, where pyruvate conversion to glucose was impaired in the absence of IL-6Ra signaling (Figure 4D). Consistent with our previous findings, we found that the effects of IL-6Ra antagonism could be fully recapitulated by using *Il6*f/f$^{\Delta UCP1}$ and *Adrb3*f/f$^{\Delta UCP1}$ animals, which lack stress-inducible IL-6 (Figures 4E and 4F). Gluconeogenic capacity is mediated by key rate-limiting enzymes, many of which have been shown to be sensitive to IL-6 signaling via STAT3 regulatory elements (Banzet et al., 2009). We thus assessed the hepatic transcriptional induction of *Pck1*, *G6pc*, and other gluconeogenic genes and found that *Pck1* and *G6pc* were significantly increased after acute stress (Figure 4G).

Please cite this article in press as: Qing et al., Origin and Function of Stress-Induced IL-6 in Murine Models, Cell (2020), https://doi.org/10.1016/j.cell.2020.05.054

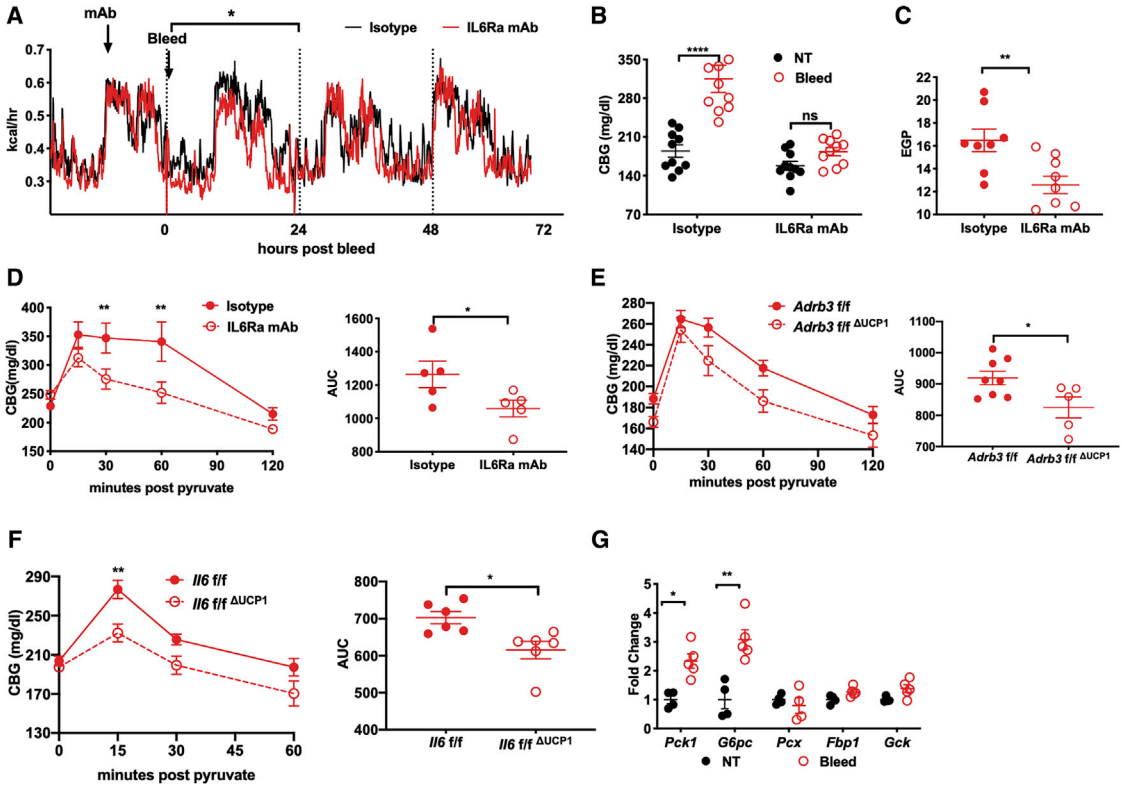

Figure 4. IL-6 is necessary for promoting stress-hyperglycemia

(A) Energy expenditure post bleeding from mice pretreated with IL-6Ra antibody or isotype control (n = 4 per group, representative of 2 experiments). Statistic represents the area under the curve (AUC) between groups.

(B) Blood glucose levels post bleeding from mice pretreated with IL-6Ra antibody or isotype control (n = 10 per group). CBG, capillary blood glucose

(C) Endogenous glucose production (EGP) post bleeding in mice pretreated with IL-6Ra antibody or isotype control (n = 8 for isotype, n = 9 for IL-6Ra monoclonal antibody [mAb]).

(D) Pyruvate tolerance test (PTT) performed 4 h after bleeding in mice pretreated with IL-6Ra antibody or isotype control (n = 5 per group, representative of 2 experiments). AUC, area under the curve.

(E and F) PTT performed 4 h after bleeding in mice with conditional *Ucp1*-mediated deletion of (E) *Adrb3* (*Adrb3*f/f$^{\Delta UCP1}$) or (F) *Il6* (*Il6*f/f$^{\Delta UCP1}$) compared respectively with their littermate controls (n = 8 for *Adrb3*f/f, n = 5 for *Adrb3*f/f$^{\Delta UCP1}$, n = 6 for *Il6*f/f or *Il6*f/f$^{\Delta UCP1}$). AUC, area under the curve.

(G) Gluconeogenesis-associated gene expression in the liver harvested 3 h post bleeding (n = 4 for NT, n = 5 for Bleed). Abbreviations are as follows: *Pck1*, phosphoenolpyruvate carboxykinase 1; *G6pc*, glucose-6-phosphatase catalytic subunit; *Pcx*, pyruvate carboxylase; *Fbp1*, fructose-1,6-bisphosphatase 1; *Gck*, glucokinase. Data are represented as mean ± SEM. *p < 0.05, **p < 0.01, ***p < 0.001, ****p < 0.0001

See also Figures S2 and S3.

Given the close crosstalk between glucose and lipid metabolism (Weickert and Pfeiffer, 2006), observations of hyperlipidemia in patients receiving anti-IL-6Ra antibodies, as well as the role of free fatty acids on hepatic glucose production (Boden et al., 1994), we studied lipid metabolism in response to acute stress. The circulating level of free fatty acids and glycerol were not significantly altered in response to retro-orbital bleeding (Figures S3A and S3B). Acute stress decreased circulating triglyceride (TG) levels (Figure S3C), which was likely a result of both enhanced TG clearance (Figure S3D) and suppressed hepatic TG production (Figure S3E). Consistent with clinical observations from patients treated with tocilizumab, anti-IL-6Ra did increase TG in the non-stressed condition (Figure S3F). However, manipulation of IL-6 signaling did not significantly impact triglyceride metabolism in response to acute stress, although stress-induced hypertriglyceridemia did trend lower in IL-6Ra antagonized animals (Figure S3F). We did not detect differences in TG, free fatty acids, glycerol, or β-hydroxybutyrate after intravenous injection of IL-6 (Figures S3H–S3K) or IL-6Ra blockade (Figure S3G), nor did we detect changes in lipolytic capacity in mice with conditional *Il6ra* deletion in adipose tissue (Figure S3L). Finally, we were unable to detect differences in *in vivo* fatty acid turnover after anti-IL-6Ra treatment (Figure S3M). Thus, we found that the dominant effect of IL-6 during acute stress is in inducing gluconeogenesis in the absence of a negative energy state to support stress-induced hyperglycemia.

IL-6Ra in the liver controls stress hyperglycemia through hepatocyte reprogramming

Because the liver and kidney are the major glucose-producing organs (Stumvoll et al., 1998), we surveyed the transcriptional induction of gluconeogenic genes in both organs and found that they were induced by bleeding stress only in the liver (Figures 5A and S4A). We observed that *Il6ra* was significantly induced

Please cite this article in press as: Qing et al., Origin and Function of Stress-Induced IL-6 in Murine Models, Cell (2020), https://doi.org/10.1016/j.cell.2020.05.054

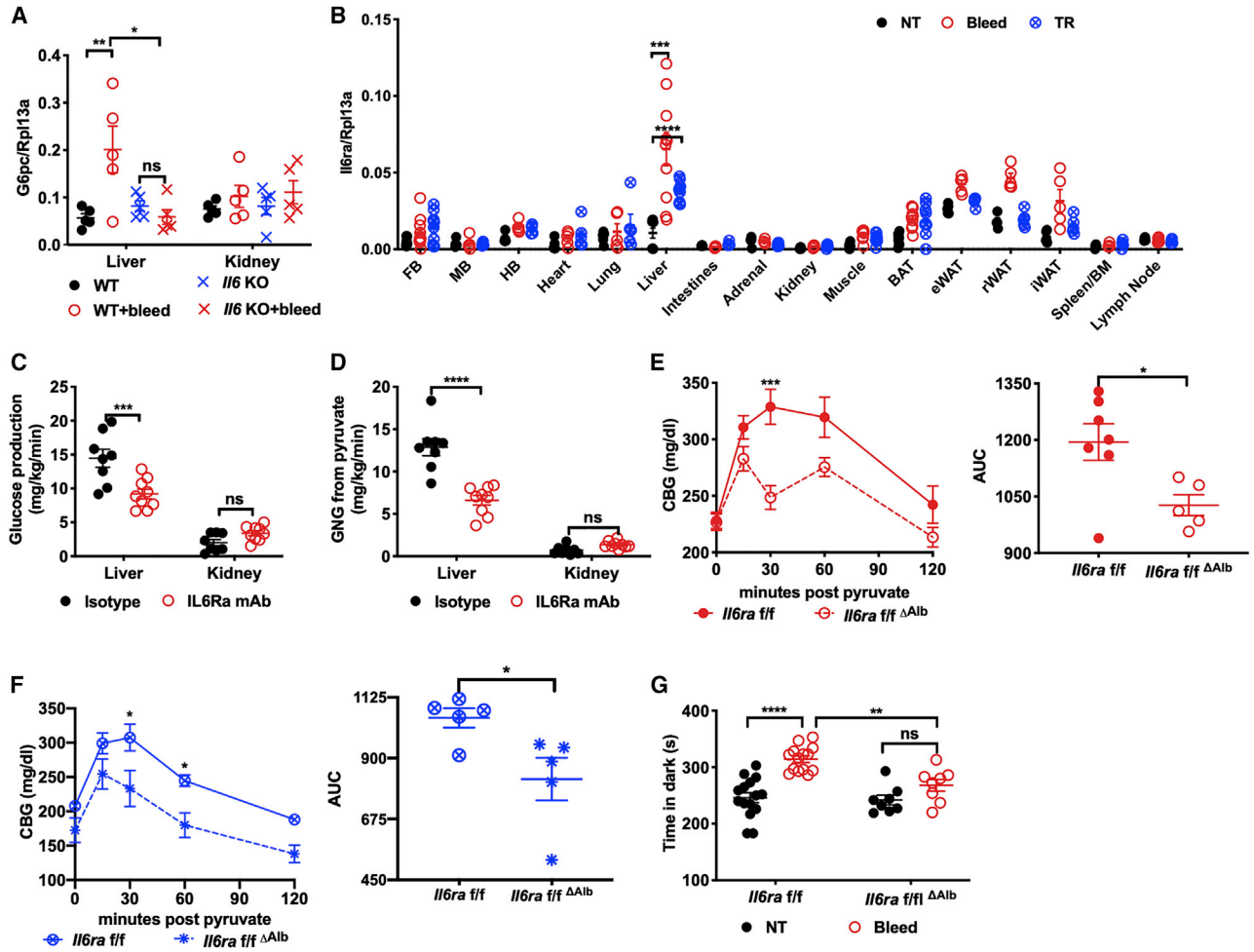

Figure 5. IL-6 mediates stress hyperglycemia through hepatocyte reprogramming

(A) *G6pc* mRNA in the liver and kidney of *Il6* KO or WT mice 4 h post bleeding (n = 5 per group).

(B) *Il6ra* mRNA in the indicated tissues from stressed mice (n = 5 per group, representative of 2 experiments). Abbreviations are as follows: FB, forebrain; MB, midbrain; HB, hindbrain; BAT, brown adipose tissue; eWAT, epididymal white adipose tissue; rWAT, retroperitoneal white adipose tissue; iWAT, inguinal white adipose tissue; NT, no treatment; TR, tube restraint.

(C and D) Rates of glucose production (C) and of gluconeogenesis (D) from pyruvate in the liver or kidney of mice treated with IL-6Ra antibody or isotype control (n = 8 for isotype, n = 9 for IL-6Ra mAb).

(E and F) PTT 4 h after bleeding (E) or tube restraint (F) in mice with hepatocyte-specific deletion of *Il6ra* (*Il6raf*/f$^{\Delta Alb}$) compared with littermate controls (*Il6raf*/f) (n = 5 per group). AUC, area under the curve.

(G) Time in the dark using the light/dark box paradigm analyzed 4 h after bleeding (bleed) from mice with hepatic deletion of *Il6ra* (*Il6raf*/f$^{\Delta Alb}$) compared with littermate controls (*Il6raf*/f) (n = 15 for *Il6raf*/f, n = 9 for *Il6raf*/f$^{\Delta Alb}$, representative of 3 experiments). Data are represented as mean ± SEM. *p < 0.05, **p < 0.01, ***p < 0.001, ****p < 0.0001.

See also Figure S4.

in liver but not in kidney (Figure 5B), suggesting that the liver might be the primary target for IL-6 signaling in response to acute stress. Concordantly, we found that the IL-6/STAT3 target genes, *Saa3* and *Socs3*, were also induced in the liver in response to acute stress (Figures S4B and S4C). To directly assess gluconeogenesis in the liver and kidney, we developed a method to assess the contribution of pyruvate to gluconeogenesis in a tissue-specific manner during stress and found that IL-6Ra antibody suppressed gluconeogenesis from pyruvate in liver but not in kidney (Figures 5C and 5D). We did not detect differences in circulating gluconeogenic amino acids (Figure S4D). Finally, to directly assess the role of hepatocyte IL-6Ra, we generated mice with hepatocyte-specific deletion of *Il6ra* (Figure S4E) and performed PTT after acute stress. We found that hepatocyte-specific deletion was sufficient to recapitulate the inhibitory effects of systemic IL-6Ra blockade on gluconeogenesis after bleeding (Figure 5E) and restraint stress (Figure 5F). These data indicate that stress-inducible IL-6 acts on the liver to induce hepatic gluconeogenesis.

We reasoned that the purpose of activating gluconeogenesis during acute stress, when animals are neither hypoglycemic nor in net-negative energy balance states, is anticipatory of

Please cite this article in press as: Qing et al., Origin and Function of Stress-Induced IL-6 in Murine Models, Cell (2020), https://doi.org/10.1016/j.cell.2020.05.054

impending increased demand ("fight or flight" response). Consequently, impairment of hepatic gluconeogenesis should be sufficient to affect adaptive behavioral responses to acute stress. To test this, we utilized the light-dark box paradigm. The light-dark box paradigm is a common tool for studying stress response behaviors where animals are placed into a novel environment in which part of the apparatus is exposed under bright light and connected to another enclosed and opaque space by a small opening (Bourin and Hascoët, 2003). In this paradigm, animals must balance the need to explore the novel space with the fear of avoiding possible predation in the exposed area. A normal adaptive response is to spend more time in the dark enclosure. We thus established baseline responses of animals with conditional hepatic deletion of *Il6ra* and then compared the responses at the peak of endocrine IL-6 after a single, conscious, retro-orbital bleed. We found that hepatic IL-6Ra was required for the normal behavioral response (Figures 5G and S4F). Taken in aggregate, we demonstrate that stress-induced IL-6 mediates stress-hyperglycemia through hepatic IL-6Ra signaling in positive energy balance states, and hepatic IL-6Ra is necessary for a normal behavioral response to acute stress.

ADRB3-dependent IL-6 from BAT potentiates lethal endotoxemia secondary to acute stress

Given the many reported roles of IL-6 in affecting inflammatory responses, we reasoned that stress-induced IL-6 might change the outcome of inflammation. We decided to use the lipopolysaccharide (LPS) model of inflammation, because in this model, mortality is due solely to the inflammatory response without any confounding contribution by pathogens. Animals were subjected to various stress models that induce IL-6 followed by a subsequent LPS challenge. We found that priming animals with stress robustly enhanced mortality to LPS (Figure 6A). For the LPS studies, we opted to use the tube-restraint model to avoid confounders associated with the hemodynamic consequences of bleeding. Because we found that ADRB3 activation was sufficient and required for stress-induced IL-6, we pre-treated animals with ADRB agonists and found that pre-treatment with ADRB3 agonist alone was sufficient to enhance LPS mortality (Figure 6B). Concordantly, a single injection of stress-dosed IL-6 was sufficient to potentiate LPS-induced mortality (Figure 6C). Because stress-induced IL-6 required consciousness, we tested whether or not animals anesthetized prior to tube restraint were still more susceptible to LPS-induced mortality and found that consciousness was required for the stress-priming effect, an effect that could be bypassed with endogenous administration of IL-6 (Figure 6D). To test if ADRB3-dependent IL-6 was necessary, ADRB3 antagonist was applied alongside the restraint challenge, which negated the effects of stress-priming (Figure 6E). Finally, we asked if *Il6*f/f$^{\Delta UCP1}$ animals, which lack stress-inducible IL-6, would be resistant to stress-priming (Figure 6F). Consistent with our hypotheses, *Il6*f/f$^{\Delta UCP1}$, which did not display altered susceptibility to LPS in the absence of stress-priming (Figure S5A), was resistant to the potentiating effects of tube-restraint on LPS mortality. We also tested the effects of stress-priming by using our *Il6ra*f/f$^{\Delta Alb}$ model. Here, regardless of stress-priming, animals lacking hepatic IL-6 signaling were significantly more sensitive to endotoxemia, suggesting that the hepatic acute phase response was a required adaptation to endotoxemia (Figure S5B), consistent with previous reports (Castell et al., 1989; Wunderlich et al., 2010). We also tested if hyperglycemia induced by IL-6 during stress was itself sufficient to prime LPS responses, and thus challenged animals to exogenous glucose to achieve stress hyperglycemia or an isocaloric isovolumetric dose of lipid, and found that glucose, but not lipid, was sufficient to prime the LPS response (Figure S5C).

To determine how stress-priming enhanced inflammation-mediated mortality, we first measured cytokine levels and tissue inflammatory gene induction. We did not detect significant changes in circulating or tissue inflammatory cytokines post-LPS in a variety of experimental settings, nor did we detect any changes in tissue inflammatory transcripts or body temperature (Figures S5D–S5R and S6D). Thus, we hypothesized that stress-induced IL-6 might be affecting host tolerance (Ferreira et al., 2011; Wang et al., 2016; Weis et al., 2017). Because our previous work isolated key brainstem functions (like maintaining heart and respiratory rate) as a target of host tolerance, we also assessed these parameters using our stress paradigm, but did not find significant differences (Figures S6A–S6F). We also did not find large differences in maintaining glycemia, fatty acid, or ketone body levels (Figures S6I–S6K), which we had previously shown to be important in host tolerance to LPS (Wang et al., 2016). Because end-organ dysfunction is a hallmark of inflammatory damage, we assessed biomarkers of vital organ function in stress-primed versus control animals and found that stress-primed animals displayed significantly more renal and a trend toward more cardiac damage, whereas hepatic damage appeared to be equivalent across conditions (Figures 6G, S6G, and S6H). These markers of end-organ damage were absent in stress-primed *Il6*f/f$^{\Delta UCP1}$ animals (Figure 6H), demonstrating that BAT-derived IL-6 from stress was required for decreasing tolerance to inflammatory damage. Together, these findings suggest that stress decreaseshost tolerance to inflammation in a BAT-derived IL-6-dependent fashion. The precise mechanism by which stress decreases host fitness to inflammation remains to be understood. Altogether, our studies suggest that stress-induced IL-6, although adaptive for supporting fight-or-flight physiology, comes at the cost of decreasing host fitness to endotoxemia-induced inflammation.

DISCUSSION

Psychological stress has been known to induce endocrine IL-6 for nearly 30 years and has been shown in multiple species, including rats, mice, and humans (Cheng et al., 2015; LeMay et al., 1990; Maes et al., 1998). However, mechanistic understanding for this phenomenon has not been addressed. The evolutionary basis for IL-6 induction during acute stress was unknown, and how this might connect to the long-observed connection between stress, metabolism, and inflammation was also unclear. Our study demonstrates that stress-induced IL-6 is produced from brown adipocytes in an ADRB3-dependent fashion in mice. Thermogenic programs were not engaged in this context, and this response was independent of ambient

Please cite this article in press as: Qing et al., Origin and Function of Stress-Induced IL-6 in Murine Models, Cell (2020), https://doi.org/10.1016/j.cell.2020.05.054

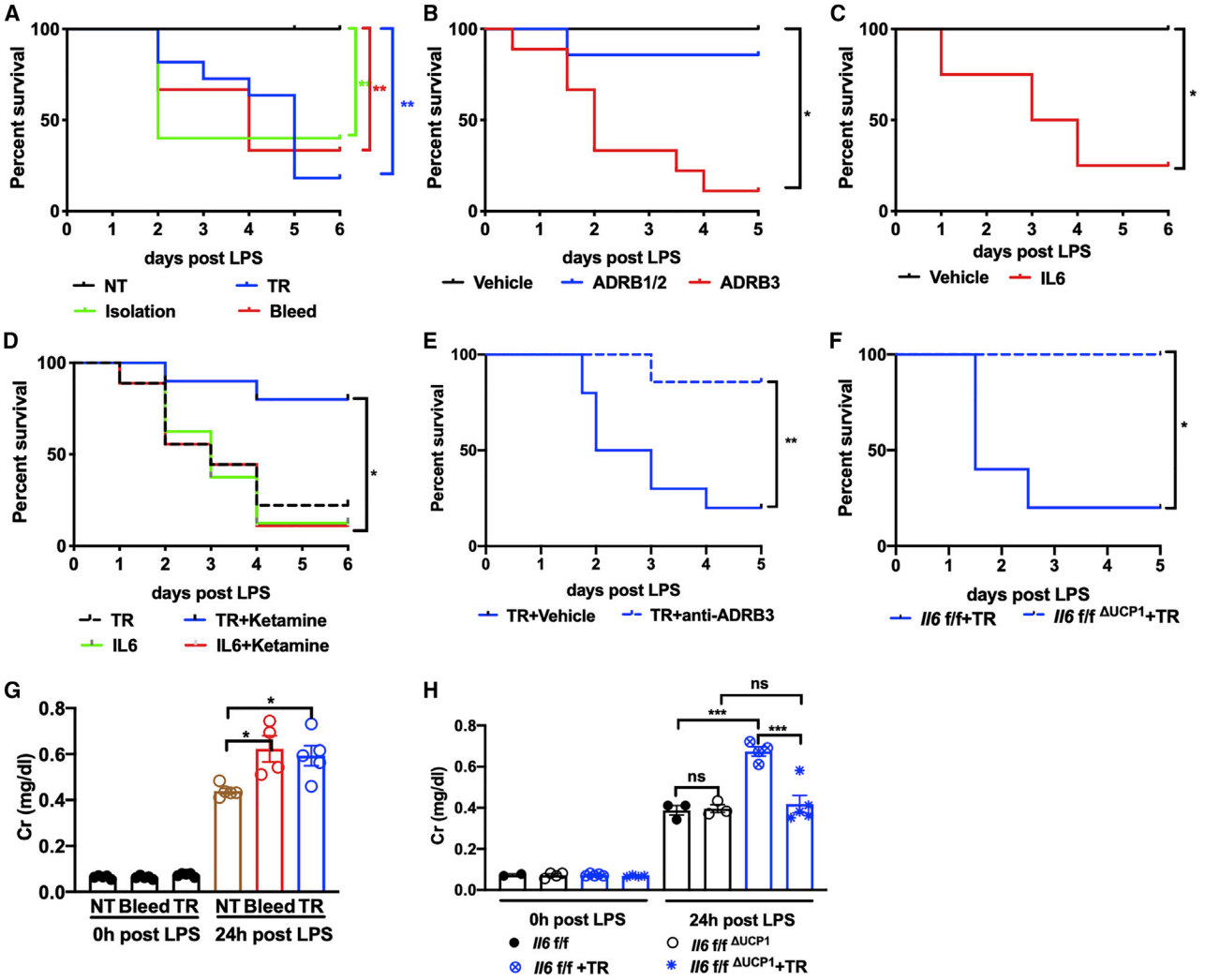

Figure 6. ADRB3-dependent IL-6 from BAT potentiates lethal endotoxemia secondary to acute stress

(A) Survival rate of LPS-induced endotoxemia in mice pre-exposed to the indicated stressors (n = 10 per group). Abbreviations are as follows: NT, no treatment; TR, tube restraint.

(B) Survival of endotoxemic animals pretreated with vehicle (n = 8), ADRB1 and ADRB2 agonist (ADRB1/2, n = 7) or ADRB3 agonist (ADRB3, n = 9).

(C) Survival of endotoxemic animals pretreated with a stress dose of IL-6 (n = 8 per group).

(D) Survival of endotoxemic animals pretreated with the indicated interventions. n = 9 for tube restraint (TR), n = 10 for TR with ketamine, n = 8 for IL-6, n = 9 for IL-6 with ketamine.

(E) Survival rate of endotoxemic mice pre-exposed to restraint with ADRB3 antagonist or vehicle injection. TR, tube restraint (n = 10 per group).

(F) Lethality in endotoxemia from mice pre-exposed to restraint with brown adipose tissue specific deletion of *Il6* (*Il6*f/f$^{\Delta UCP1}$) compared with littermate controls (*Il6*f/f) (n = 10 per group).

(G) Circulating creatinine (Cr) levels 0 or 24 h post LPS injection from mice pre-exposed to bleeding or restraint stress (n = 5 per group). Abbreviations are as follows: NT, no treatment; TR, tube restraint.

(H) Circulating creatinine (Cr) levels 0 or 24 h post LPS injection from mice pre-exposed to restraint stress with brown adipose tissue specific deletion of *Il6* (*Il6*f/f$^{\Delta UCP1}$) compared with littermate controls (*Il6*f/f) (n = 5 per group). TR, tube restraint. Data are represented as mean ± SEM. *p < 0.05, **p < 0.01, ***p < 0.001, ****p < 0.0001

See also Figures S5 and S6.

temperature. One key role of stress-induced endocrine IL-6 is in reprogramming organismal metabolism by instructing hepatic gluconeogenesis in the absence of a net negative energy balance or hypoglycemic state, likely in anticipation of increased glucose demand. Hepatic IL-6 signaling was also necessary for mediating normal behavioral responses in the light-dark box paradigm suggesting that hepatic organismal reprogramming is required for an adaptive "fight or flight" response. Finally, we found that stress-induced BAT-derived endocrine IL-6 was necessary and sufficient for decreasing host tolerance to a subsequent inflammatory response by using the endotoxemia model.

Please cite this article in press as: Qing et al., Origin and Function of Stress-Induced IL-6 in Murine Models, Cell (2020), https://doi.org/10.1016/j.cell.2020.05.054

Gluconeogenesis is normally not engaged in positive energy balance states, with the exception of forced exercise (Banzet et al., 2009). In this setting, IL-6 is derived from myocytes and induces hepatic gluconeogenesis. In our study, we did not observe any IL-6 induction in muscle, nor did we observe increased activity after stress, and instead found that brown adipocytes were indispensable in the setting of acute stress. It is interesting to speculate why IL-6, which can be derived from many different cell types, is produced by brown adipocytes in this context. The BAT has a number of features that make it an ideal endocrine organ responsive to acute psychologic stress. It is highly innervated, and thus capable of immediate responsiveness after detection of stress, a feature that has been clearly demonstrated in acute cold exposure for the purpose of defending body temperature. In addition, blood flow through BAT can be quickly increased (hyperemia) (Abreu-Vieira et al., 2015) and, in the setting of acute cold exposure, is optimal for quickly circulating warmed blood, or, in this case, a stress hormone. Interestingly, BAT hyperemia and thermogenesis can be decoupled, suggesting that there could be scenarios where uncoupled respiration is not necessary for hyperemia (Abreu-Vieira et al., 2015). In our study, we did not find that ambient temperature played a role in stress-inducible IL-6, observe transcriptional induction of the thermogenic program, find differences in body temperature as a function of IL-6 signaling, or demonstrate a requirement for UCP1. We speculate that perhaps through other contextual inputs, such as the cold-sensor TRPM8 (Ma et al., 2012; Moraes et al., 2017), might be required to activate the full thermogenic program. From this perspective, BAT can thus be considered a stress-responsive endocrine organ that might have several responses depending on other contextual inputs. Finally, BAT is highly enriched in ADRB3. Unlike ADRB1 or ADRB2, ADRB3 has been shown to be less easily desensitized (Rouget et al., 2004), thus providing more durable responsiveness to adrenergic outflow. Consistent with this idea, we found that repeated stress-exposure over the course of 24 h maintained elevated plasma IL-6 levels. The role of BAT in adult humans is controversial because its detection is dependent upon the approach employed (Leitner et al., 2017; Porter et al., 2016; van Marken Lichtenbelt et al., 2009). It is principally confined to clavicular and para-aortic areas, which might be why less stress-associated IL-6 is recovered in humans than in mice if it is even made in human BAT at all (Maes et al., 1998). On the other hand, recent work suggests that BAT of "humanized" mice is notably similar to human BAT (de Jong et al., 2019). It remains unclear how the mechanistic insights from our studies in rodents will translate to humans.

Our work further highlights the complexity of adrenergic signaling in physiology. Although signaling on ADRB2 in immune cells has largely been shown to be anti-inflammatory (Ağaç et al., 2018; Nance and Sanders, 2007), our study suggests that ADRB3 activation after acute stress exposure might be detrimental for adaptation to a subsequent inflammatory challenge. The clinical observation that sympathetic mimetics enhance survival in septic shock might be resultant from the effects of supraphysiological dosing on supporting blood pressure that might be the dominant mechanism of protection regardless of its other effects.

Like adrenergic biology, the role of IL-6 in inflammation and metabolism is similarly complex. IL-6 is generally considered a pro-inflammatory cytokine, which is supported by the efficacy of IL-6 blockade in inflammatory diseases (Kotch et al., 2019). On the other hand, several studies demonstrate an anti-inflammatory role for IL-6 (Mauer et al., 2014; Nandi et al., 2010). In our study, we demonstrate that BAT-derived IL-6 is required for stress to enhance end-organ damage and mortality caused by the LPS model. Likewise, we found that pre-exposure to peak plasma levels of stress-induced IL-6 was sufficient to increase end-organ damage and potentiate mortality. In the LPS model, which might not be generalizable to other models of inflammation, we found that although stress did not meaningfully increase inflammatory magnitude, hemodynamic or cardiopulmonary parameters, or gross metabolic parameters, it nonetheless led to measurable worsening of end-organ function and death. The mechanism underlying this phenomenon is unclear, but likely is a result of stress-induced IL-6-dependent metabolic re-programming similar to that which has been previously published by our group and others (Ganeshan et al., 2019; Luan et al., 2019; Wang et al., 2016; Luan et al., 2019; Weis et al., 2017). Whether other types of inflammatory challenges would also be affected by the models of acute stress used here, and, more generally, how different types, degrees, and durations of stress affect tissue tolerance in different inflammatory settings is an open question, as is the precise mechanism for how IL-6 primes LPS-mediated mortality. Moreover, it remains unclear if the elevated levels of circulating IL-6 seen in aging and obesity or after exercise would also drive differences in host tolerance to inflammation. Similarly, from a metabolic perspective, IL-6 has been shown to be both insulin sensitizing and insulin desensitizing depending on the context. In contexts of chronically increased IL-6 such as obesity or rheumatoid arthritis, IL-6 has been shown to induce insulin resistance (Castañeda et al., 2019; Kim et al., 2004; Perry et al., 2015). On the other hand, in these same contexts, others have shown that IL-6 induces insulin sensitivity (Carey et al., 2006; Findeisen et al., 2019; Matthews et al., 2010; Mauer et al., 2014; Steensberg et al., 2003; Timper et al., 2017), whereas IL-6 has been shown to be insulin sensitizing in exercise (Benrick et al., 2012). Our study did not find that IL-6 was playing a role in insulin sensitivity after stress. Our animals were all lean, chow-fed animals, and thus in a net energy positive state. One main finding of our study is that IL-6 is a distinct inductive signal to instruct hepatic gluconeogenesis during net energy positive states. Unlike during fasting, ketogenic diets, or other hypoglycemic states where gluconeogenesis programs are mediated primarily by CREB/FoxO1 programs (Oh et al., 2013), which are responsive to low energy states, stress induces gluconeogenesis even in net positive energy balance states. Our data suggest that IL-6 signaling in hepatocytes is required for gluconeogenesis in non-net negative energy balance states. Although IL-6 does not appear to increase gluconeogenesis at rest (Steensberg et al., 2003), our studies resonate well with other studies demonstrating STAT3 regulation of the same gluconeogenic genes such as *Pck1* and *G6pc* and with studies demonstrating a role for IL-6 in exercise-mediated hepatic gluconeogenesis (Banzet et al., 2009). Here, it is interesting to consider the similarities between psychological stress and

Please cite this article in press as: Qing et al., Origin and Function of Stress-Induced IL-6 in Murine Models, Cell (2020), https://doi.org/10.1016/j.cell.2020.05.054

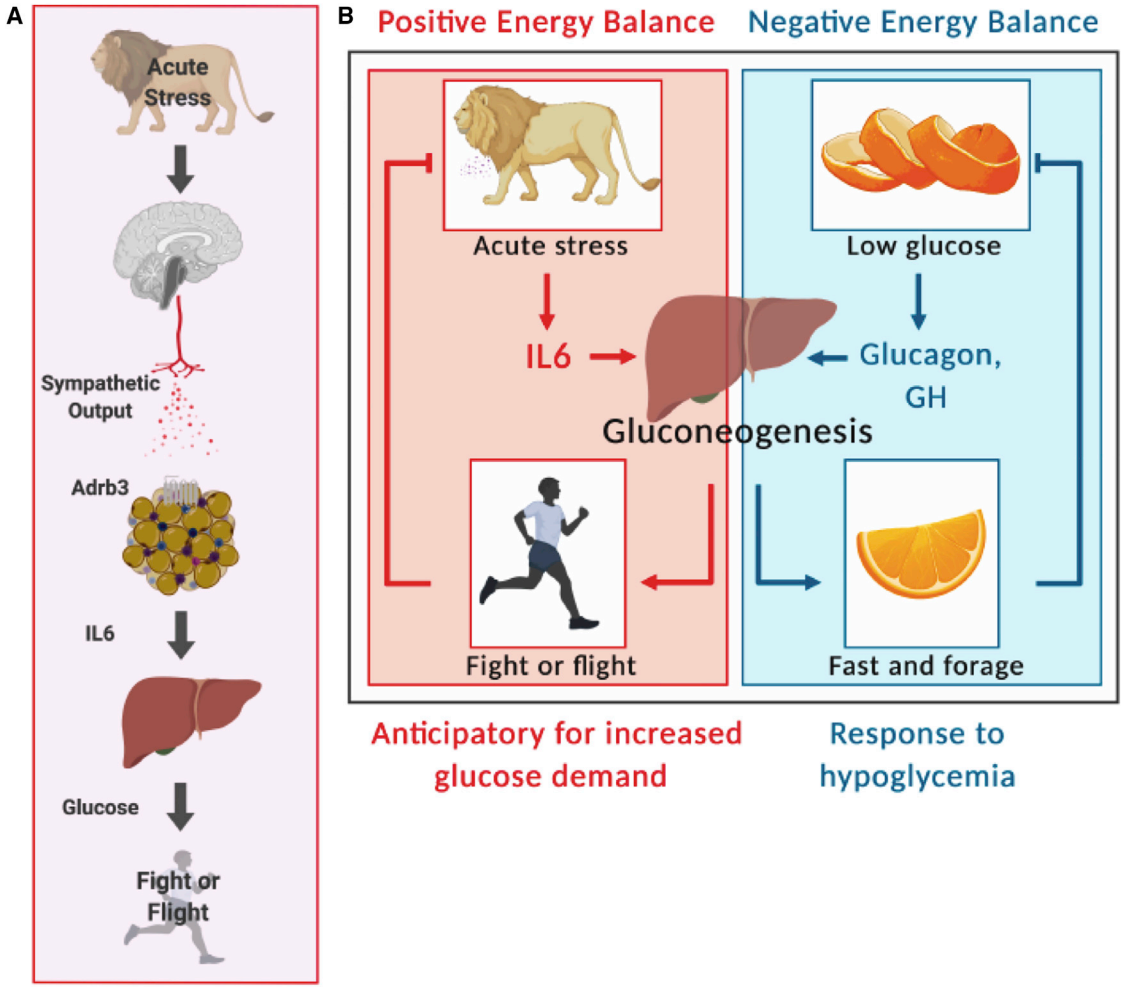

Figure 7. Model

(A) Acute stresses engage a brain-BAT-liver axis to promote metabolic adaptation in order to support fight or flight physiology.

(B) Acute stress, unlike fasting or other negative energy states, requires IL-6, in contrast to hormones like glucagon or growth hormone (GH), to induce gluconeogenesis for anticipatory (impending increase in glucose demand), as opposed to responsive adaptation.

forced exercise. Thus, we propose a model wherein IL-6 is a necessary signal that instructs gluconeogenesis in net energy positive states as an anticipatory, (impending increase in glucose demand), as opposed to responsive adaptation (Figure 7).

We found that hepatic IL-6 signaling was required for a normal behavioral adaptation to stress. Numerous studies have reported that intracranial IL-6 and IL-6 signaling by using non-canonical *trans*-signaling modalities impact behavior (Rothaug et al., 2016). Our findings that hepatocyte expression of *Il6ra* is required for normal behavioral response to acute stress are in line with recent studies using chronic models of stress (Hodes et al., 2014; Niraula et al., 2019; Zhang et al., 2017), where the use of blocking antibodies to IL-6Ra, which do not cross the blood brain barrier (Nellan et al., 2018), promoted resilience to social stress. These studies suggest a necessary peripheral role for IL-6 in mediating behavioral changes, consistent with our findings. It is possible that hepatocyte IL-6Ra would be required in these models of chronic stress as well. Indeed, the light-dark box paradigm we utilized in this study is commonly used in depression and anxiety studies, and IL-6 has been implicated in depression for many years (Kappelmann et al., 2018). On the other hand, aerobic exercise, which also induces IL-6 (Benrick et al., 2012; Pedersen and Febbraio, 2008; Reza et al., 2017), is highly associated with improved outcomes in depression and anxiety. Thus, it remains to be seen in on-going clinical trials (i.e., NCT02660528) if elevated IL-6 observed in depressed patients is pathogenic.

Our studies suggest that the degree of stress experienced by an animal at the time of inflammatory challenge might be one important factor for determining its disease trajectory. Understanding which environmental factors—such as timing to the last meal bolus or other determinants that are proxies for the "stressfulness" of the environment—might contribute to the stochasticity observed in genetically identical organisms subjected to identical challenges, which is an area of active study that

might shed insight into mechanistic determinants of disease trajectories.

In summary, this study identifies a brain-BAT-liver axis in mice whereby IL-6 modulates glucose metabolism under conditions of acute stress and suggests that there is an adaptive purpose for inducing IL-6 in acute stress. We speculate that maladaptive states might arise in chronic stress where IL-6 becomes persistently elevated. Whether or not ADRB3 or IL-6Ra receptor biology changes as a function of chronic IL-6 states, as has been shown for the glucocorticoid and insulin receptors (Boucher et al., 2014; Cohen et al., 2012), remains to be seen. Should this brain-BAT-liver axis also be relevant in humans, our findings have implications for the pathogenesis of psychiatric diseases such as seasonal affective disorder, where depression occurs primarily as a function of cold and dark seasons, and also implicate ADRB3 and IL-6 as potential therapeutic targets for preventing disease flares in conditions of pathologic inflammation.

Limitations of study

These experiments were performed on mice in a single facility and largely on the C57BL/6J genetic background. The impact of the microbiota, genetic background, and facility-specific factors are unknown, and the unnatural settings in animal facilities likely affect the results and interpretation of physiology studies, including this one. It is likely that stress-induced IL-6 plays additional roles besides those described in our studies. There are a number of open questions raised by our study. Does psychological stress affect all types of inflammation the same? How do different stressors and degrees of stress affect inflammation? Are our observations informative for placebo and nocebo biology? Finally, the translatability of this study to humans is to be determined.

STAR★METHODS

Detailed methods are provided in the online version of this paper and include the following:

SUPPLEMENTAL INFORMATION

Supplemental Information can be found online at https://doi.org/10.1016/j.cell.2020.05.054.

ACKNOWLEDGMENTS

We thank members of the Wang, Picciotto, Sinha, and Perry labs for helpful discussions. We are indebted to Dr. Ruslan Medzhitov for his guidance and support. We thank Ali Nasiri and Wanling Zhu for the mouse metabolic flux phenotyping, Dr. Mamula's lab for sharing equipment, and Dr. Akiko Iwasaki for use of thermoneutral cabinets. We thank Mrs. Krista Wang, Dr. Ruth Franklin, and Dr. Harding Luan for review of the manuscript. Invasive hemodynamic monitoring was performed through the George M. O'Brien Kidney Center at Yale (NIH P30-DK079310). A.W. was supported by the NIH Clinical Investigator Award (K08AI128745). K.I.-W. was supported by a Gruber Fellowship. Metabolic flux analysis performed in the Perry lab was supported by an NIH Pathway to Independence Award (K99/R00 CA215315) to R.J.P. M.R.P. was supported by NIH grants DA050986, MH077681, and DA14241. R.S. was supported by NIH grant R01-DK099039.

AUTHOR CONTRIBUTIONS

H.Q. and R.D. contributed equally to this work. H.Q., R.D., and A.W. designed the study, analyzed the data, and wrote the manuscript with input from the other authors. H.Q. and R.D. performed the experiments with assistance from K.I.-W. and C.Z. R.J.P. performed all analyses for flux studies. S.R. in the laboratory of N.W.P. assisted with experiments with gnotobiotic animals. N.F. in the laboratory of R.S. collected all human samples, performed the analyses, and provided input into stress biology. Y.M., in the laboratory of M.R.P. provided assistance with behavioral studies.

DECLARATION OF INTERESTS

The authors declare no competing interests.

Received: August 26, 2019
Revised: March 16, 2020
Accepted: May 28, 2020
Published: June 30, 2020

REFERENCES

Abreu-Vieira, G., Hagberg, C.E., Spalding, K.L., Cannon, B., and Nedergaard, J. (2015). Adrenergically stimulated blood flow in brown adipose tissue is not dependent on thermogenesis. Am. J. Physiol. Endocrinol. Metab. *308*, E822–E829.

Ağaç, D., Estrada, L.D., Maples, R., Hooper, L.V., and Farrar, J.D. (2018). The β2-adrenergic receptor controls inflammation by driving rapid IL-10 secretion. Brain Behav. Immun. *74*, 176–185.

Ansell, E.B., Rando, K., Tuit, K., Guarnaccia, J., and Sinha, R. (2012). Cumulative adversity and smaller gray matter volume in medial prefrontal, anterior cingulate, and insula regions. Biol. Psychiatry *72*, 57–64.

Aune, U.L., Ruiz, L., and Kajimura, S. (2013). Isolation and differentiation of stromal vascular cells to beige/brite cells. J. Vis. Exp. (73), 50191.

Banzet, S., Koulmann, N., Simler, N., Sanchez, H., Chapot, R., Serrurier, B., Peinnequin, A., and Bigard, X. (2009). Control of gluconeogenic genes during intense/prolonged exercise: hormone-independent effect of muscle-derived IL-6 on hepatic tissue and PEPCK mRNA. J. Appl. Physiol. (1985) *107*, 1830–1839.

Batty, G.D., Russ, T.C., Stamatakis, E., and Kivimaki, M. (2017). Psychological distress in relation to site specific cancer mortality: pooling of unpublished data from 16 prospective cohort studies. BMJ *356*, j108.

Benrick, A., Wallenius, V., and Asterholm, I.W. (2012). Interleukin-6 mediates exercise-induced increase in insulin sensitivity in mice. Exp. Physiol. *97*, 1224–1235.

Bethin, K.E., Vogt, S.K., and Muglia, L.J. (2000). Interleukin-6 is an essential, corticotropin-releasing hormone-independent stimulator of the adrenal axis during immune system activation. Proc. Natl. Acad. Sci. USA *97*, 9317–9322.

Black, D.S., and Slavich, G.M. (2016). Mindfulness meditation and the immune system: a systematic review of randomized controlled trials. Ann. N Y Acad. Sci. *1373*, 13–24.

Boden, G., Chen, X., Ruiz, J., White, J.V., and Rossetti, L. (1994). Mechanisms of fatty acid-induced inhibition of glucose uptake. J. Clin. Invest. *93*, 2438–2446.

Boucher, J., Kleinridders, A., and Kahn, C.R. (2014). Insulin receptor signaling in normal and insulin-resistant states. Cold Spring Harb. Perspect. Biol. *6*, a009191.

Bourin, M., and Hascoët, M. (2003). The mouse light/dark box test. Eur. J. Pharmacol. *463*, 55–65.

Carey, A.L., Steinberg, G.R., Macaulay, S.L., Thomas, W.G., Holmes, A.G., Ramm, G., Prelovsek, O., Hohnen-Behrens, C., Watt, M.J., James, D.E., et al. (2006). Interleukin-6 increases insulin-stimulated glucose disposal in humans and glucose uptake and fatty acid oxidation in vitro via AMP-activated protein kinase. Diabetes *55*, 2688–2697.

Castañeda, S., Remuzgo-Martínez, S., López-Mejías, R., Genre, F., Calvo-Alén, J., Llorente, I., Aurrecoechea, E., Ortiz, A.M., Triguero, A., Blanco, R., et al. (2019). Rapid beneficial effect of the IL-6 receptor blockade on insulin resistance and insulin sensitivity in non-diabetic patients with rheumatoid arthritis. Clin. Exp. Rheumatol. *37*, 465–473.

Castell, J.V., Gómez-Lechón, M.J., David, M., Andus, T., Geiger, T., Trullenque, R., Fabra, R., and Heinrich, P.C. (1989). Interleukin-6 is the major regulator of acute phase protein synthesis in adult human hepatocytes. FEBS Lett. *242*, 237–239.

Cheng, Y., Jope, R.S., and Beurel, E. (2015). A pre-conditioning stress accelerates increases in mouse plasma inflammatory cytokines induced by stress. BMC Neurosci. *16*, 31.

Chowdhury, S., Schulz, L., Palmisano, B., Singh, P., Berger, J.M., Yadav, V.K., Mera, P., Ellingsgaard, H., Hidalgo, J., Brüning, J., and Karsenty, G. (2020). Muscle-derived Interleukin 6 Increases Exercise Capacity by Signaling in Osteoblasts. J. Clin. Invest. *130*, 2888–2902.

Cohen, S., Janicki-Deverts, D., Doyle, W.J., Miller, G.E., Frank, E., Rabin, B.S., and Turner, R.B. (2012). Chronic stress, glucocorticoid receptor resistance, inflammation, and disease risk. Proc. Natl. Acad. Sci. USA *109*, 5995–5999.

Covarrubias, A.J., and Horng, T. (2014). IL-6 strikes a balance in metabolic inflammation. Cell Metab. *19*, 898–899.

de Jong, J.M.A., Sun, W., Pires, N.D., Frontini, A., Balaz, M., Jespersen, N.Z., Feizi, A., Petrovic, K., Fischer, A.W., Bokhari, M.H., et al. (2019). Human brown adipose tissue is phenocopied by classical brown adipose tissue in physiologically humanized mice. Nat. Metab. *1*, 830–843.

Depocas, F., Foster, D.O., Zaror-Behrens, G., Lacelle, S., and Nadeau, B. (1984). Recovery of function in sympathetic nerves of interscapular brown adipose tissue of rats treated with 6-hydroxydopamine. Can. J. Physiol. Pharmacol. *62*, 1327–1332.

Eisner, M.D., Katz, P.P., Lactao, G., and Iribarren, C. (2005). Impact of depressive symptoms on adult asthma outcomes. Ann. Allergy Asthma Immunol. *94*, 566–574.

Esposito, K., Nappo, F., Marfella, R., Giugliano, G., Giugliano, F., Ciotola, M., Quagliaro, L., Ceriello, A., and Giugliano, D. (2002). Inflammatory cytokine concentrations are acutely increased by hyperglycemia in humans: role of oxidative stress. Circulation *106*, 2067–2072.

Febbraio, M.A., Hiscock, N., Sacchetti, M., Fischer, C.P., and Pedersen, B.K. (2004). Interleukin-6 is a novel factor mediating glucose homeostasis during skeletal muscle contraction. Diabetes *53*, 1643–1648.

Felger, J.C., and Lotrich, F.E. (2013). Inflammatory cytokines in depression: neurobiological mechanisms and therapeutic implications. Neuroscience *246*, 199–229.

Ferreira, A., Marguti, I., Bechmann, I., Jeney, V., Chora, A., Palha, N.R., Rebelo, S., Henri, A., Beuzard, Y., and Soares, M.P. (2011). Sickle hemoglobin confers tolerance to Plasmodium infection. Cell *145*, 398–409.

Findeisen, M., Allen, T.L., Henstridge, D.C., Kammoun, H., Brandon, A.E., Baggio, L.L., Watt, K.I., Pal, M., Cron, L., Estevez, E., et al. (2019). Treatment of type 2 diabetes with the designer cytokine IC7Fc. Nature *574*, 63–68.

Frank, M.G., Watkins, L.R., and Maier, S.F. (2013). Stress-induced glucocorticoids as a neuroendocrine alarm signal of danger. Brain Behav. Immun. *33*, 1–6.

Ganeshan, K., Nikkanen, J., Man, K., Leong, Y.A., Sogawa, Y., Maschek, J.A., Van Ry, T., Chagwedera, D.N., Cox, J.E., and Chawla, A. (2019). Energetic Trade-Offs and Hypometabolic States Promote Disease Tolerance. Cell *177*, 399–413.

Gao, Y., Liu, F., Fang, L., Cai, R., Zong, C., and Qi, Y. (2014). Genkwanin inhibits proinflammatory mediators mainly through the regulation of miR-101/MKP-1/MAPK pathway in LPS-activated macrophages. PLoS ONE *9*, e96741.

Greenhill, C.J., Rose-John, S., Lissilaa, R., Ferlin, W., Ernst, M., Hertzog, P.J., Mansell, A., and Jenkins, B.J. (2011). IL-6 trans-signaling modulates TLR4-dependent inflammatory responses via STAT3. J. Immunol. *186*, 1199–1208.

Hippocrates. (1849). The genuine works of Hippocrates/translated from the Greek, with a preliminary discourse and annotations by Francis Adams, in two volumes (The Sydenham Society).

Hodes, G.E., Pfau, M.L., Leboeuf, M., Golden, S.A., Christoffel, D.J., Bregman, D., Rebusi, N., Heshmati, M., Aleyasin, H., Warren, B.L., et al. (2014). Individual differences in the peripheral immune system promote resilience versus susceptibility to social stress. Proc. Natl. Acad. Sci. USA *111*, 16136–16141.

Hunter, C.A., and Jones, S.A. (2015). IL-6 as a keystone cytokine in health and disease. Nat. Immunol. *16*, 448–457.

Kappelmann, N., Lewis, G., Dantzer, R., Jones, P.B., and Khandaker, G.M. (2018). Antidepressant activity of anti-cytokine treatment: a systematic review and meta-analysis of clinical trials of chronic inflammatory conditions. Mol. Psychiatry *23*, 335–343.

Kataoka, N., Hioki, H., Kaneko, T., and Nakamura, K. (2014). Psychological stress activates a dorsomedial hypothalamus-medullary raphe circuit driving brown adipose tissue thermogenesis and hyperthermia. Cell Metab. *20*, 346–358.

Kawate, R., Talan, M.I., and Engel, B.T. (1994). Sympathetic nervous activity to brown adipose tissue increases in cold-tolerant mice. Physiol. Behav. *55*, 921–925.

Kelly, J.R., Kennedy, P.J., Cryan, J.F., Dinan, T.G., Clarke, G., and Hyland, N.P. (2015). Breaking down the barriers: the gut microbiome, intestinal permeability and stress-related psychiatric disorders. Front. Cell. Neurosci. *9*, 392.

Khandaker, G.M., Pearson, R.M., Zammit, S., Lewis, G., and Jones, P.B. (2014). Association of serum interleukin 6 and C-reactive protein in childhood with depression and psychosis in young adult life: a population-based longitudinal study. JAMA Psychiatry *71*, 1121–1128.

Khokha, R., Murthy, A., and Weiss, A. (2013). Metalloproteinases and their natural inhibitors in inflammation and immunity. Nat. Rev. Immunol. *13*, 649–665.

Kim, H.J., Higashimori, T., Park, S.Y., Choi, H., Dong, J., Kim, Y.J., Noh, H.L., Cho, Y.R., Cline, G., Kim, Y.B., and Kim, J.K. (2004). Differential effects of interleukin-6 and -10 on skeletal muscle and liver insulin action in vivo. Diabetes *53*, 1060–1067.

Kosteli, A., Sugaru, E., Haemmerle, G., Martin, J.F., Lei, J., Zechner, R., and Ferrante, A.W., Jr. (2010). Weight loss and lipolysis promote a dynamic immune response in murine adipose tissue. J. Clin. Invest. *120*, 3466–3479.

Kotch, C., Barrett, D., and Teachey, D.T. (2019). Tocilizumab for the treatment of chimeric antigen receptor T cell-induced cytokine release syndrome. Expert Rev. Clin. Immunol. *15*, 813–822.

Lee, M.W., Odegaard, J.I., Mukundan, L., Qiu, Y., Molofsky, A.B., Nussbaum, J.C., Yun, K., Locksley, R.M., and Chawla, A. (2015). Activated type 2 innate lymphoid cells regulate beige fat biogenesis. Cell *160*, 74–87.

Leitner, B.P., Huang, S., Brychta, R.J., Duckworth, C.J., Baskin, A.S., McGehee, S., Tal, I., Dieckmann, W., Gupta, G., Kolodny, G.M., et al. (2017). Mapping of human brown adipose tissue in lean and obese young men. Proc. Natl. Acad. Sci. USA *114*, 8649–8654.

LeMay, L.G., Vander, A.J., and Kluger, M.J. (1990). The effects of psychological stress on plasma interleukin-6 activity in rats. Physiol. Behav. *47*, 957–961.

Liu, L.Y., Coe, C.L., Swenson, C.A., Kelly, E.A., Kita, H., and Busse, W.W. (2002). School examinations enhance airway inflammation to antigen challenge. Am. J. Respir. Crit. Care Med. *165*, 1062–1067.

Liu, Y.Z., Wang, Y.X., and Jiang, C.L. (2017). Inflammation: The Common Pathway of Stress-Related Diseases. Front. Hum. Neurosci. *11*, 316.

Luan, H.H., Wang, A., Hilliard, B.K., Carvalho, F., Rosen, C.E., Ahasic, A.M., Herzog, E.L., Kang, I., Pisani, M.A., Yu, S., et al. (2019). GDF15 Is an Inflammation-Induced Central Mediator of Tissue Tolerance. Cell *178*, 1231–1244.

Ma, S., Yu, H., Zhao, Z., Luo, Z., Chen, J., Ni, Y., Jin, R., Ma, L., Wang, P., Zhu, Z., et al. (2012). Activation of the cold-sensing TRPM8 channel triggers UCP1-dependent thermogenesis and prevents obesity. J. Mol. Cell Biol. *4*, 88–96.

Maes, M., Song, C., Lin, A., De Jongh, R., Van Gastel, A., Kenis, G., Bosmans, E., De Meester, I., Benoy, I., Neels, H., et al. (1998). The effects of psychological stress on humans: increased production of pro-inflammatory cytokines and a Th1-like response in stress-induced anxiety. Cytokine *10*, 313–318.

Masuda, K., Ripley, B., Nishimura, R., Mino, T., Takeuchi, O., Shioi, G., Kiyonari, H., and Kishimoto, T. (2013). Arid5a controls IL-6 mRNA stability, which contributes to elevation of IL-6 level in vivo. Proc. Natl. Acad. Sci. USA *110*, 9409–9414.

Matthews, V.B., Allen, T.L., Risis, S., Chan, M.H., Henstridge, D.C., Watson, N., Zaffino, L.A., Babb, J.R., Boon, J., Meikle, P.J., et al. (2010). Interleukin-6-deficient mice develop hepatic inflammation and systemic insulin resistance. Diabetologia *53*, 2431–2441.

Mauer, J., Chaurasia, B., Goldau, J., Vogt, M.C., Ruud, J., Nguyen, K.D., Theurich, S., Hausen, A.C., Schmitz, J., Brönneke, H.S., et al. (2014). Signaling by IL-6 promotes alternative activation of macrophages to limit endotoxemia and obesity-associated resistance to insulin. Nat. Immunol. *15*, 423–430.

Mineur, Y.S., Somenzi, O., and Picciotto, M.R. (2007). Cytisine, a partial agonist of high-affinity nicotinic acetylcholine receptors, has antidepressant-like properties in male C57BL/6J mice. Neuropharmacology *52*, 1256–1262.

Mohr, D.C., Hart, S.L., Julian, L., Cox, D., and Pelletier, D. (2004). Association between stressful life events and exacerbation in multiple sclerosis: a meta-analysis. BMJ *328*, 731.

Moraes, M.N., de Assis, L.V.M., Henriques, F.D.S., Batista, M.L., Jr., Güler, A.D., and Castrucci, A.M.L. (2017). Cold-sensing TRPM8 channel participates in circadian control of the brown adipose tissue. Biochim. Biophys. Acta Mol. Cell Res. *1864*, 2415–2427.

Munck, A., Guyre, P.M., and Holbrook, N.J. (1984). Physiological functions of glucocorticoids in stress and their relation to pharmacological actions. Endocr. Rev. *5*, 25–44.

Nance, D.M., and Sanders, V.M. (2007). Autonomic innervation and regulation of the immune system (1987-2007). Brain Behav. Immun. *21*, 736–745.

Nandi, D., Mishra, M.K., Basu, A., and Bishayi, B. (2010). Protective effects of interleukin-6 in lipopolysaccharide (LPS)-induced experimental endotoxemia are linked to alteration in hepatic anti-oxidant enzymes and endogenous cytokines. Immunobiology *215*, 443–451.

Nellan, A., McCully, C.M.L., Cruz Garcia, R., Jayaprakash, N., Widemann, B.C., Lee, D.W., and Warren, K.E. (2018). Improved CNS exposure to tocilizumab after cerebrospinal fluid compared to intravenous administration in rhesus macaques. Blood *132*, 662–666.

Nguyen, N.L., Barr, C.L., Ryu, V., Cao, Q., Xue, B., and Bartness, T.J. (2017). Separate and shared sympathetic outflow to white and brown fat coordinately regulates thermoregulation and beige adipocyte recruitment. Am. J. Physiol. Regul. Integr. Comp. Physiol. *312*, R132–R145.

Niraula, A., Witcher, K.G., Sheridan, J.F., and Godbout, J.P. (2019). Interleukin-6 Induced by Social Stress Promotes a Unique Transcriptional Signature in the Monocytes That Facilitate Anxiety. Biol. Psychiatry *85*, 679–689.

Oh, K.J., Han, H.S., Kim, M.J., and Koo, S.H. (2013). CREB and FoxO1: two transcription factors for the regulation of hepatic gluconeogenesis. BMB Rep. *46*, 567–574.

Osuchowski, M.F., Welch, K., Siddiqui, J., and Remick, D.G. (2006). Circulating cytokine/inhibitor profiles reshape the understanding of the SIRS/CARS continuum in sepsis and predict mortality. J. Immunol. *177*, 1967–1974.

Päth, G., Scherbaum, W.A., and Bornstein, S.R. (2000). The role of interleukin-6 in the human adrenal gland. Eur. J. Clin. Invest. *30* (*Suppl 3*), 91–95.

Pbert, L., Madison, J.M., Druker, S., Olendzki, N., Magner, R., Reed, G., Allison, J., and Carmody, J. (2012). Effect of mindfulness training on asthma quality of life and lung function: a randomised controlled trial. Thorax *67*, 769–776.

Pedersen, B.K., and Febbraio, M.A. (2007). Point: Interleukin-6 does have a beneficial role in insulin sensitivity and glucose homeostasis. J. Appl. Physiol. (1985) *102*, 814–816.

Pedersen, B.K., and Febbraio, M.A. (2008). Muscle as an endocrine organ: focus on muscle-derived interleukin-6. Physiol. Rev. *88*, 1379–1406.

Perry, R.J., Camporez, J.G., Kursawe, R., Titchenell, P.M., Zhang, D., Perry, C.J., Jurczak, M.J., Abudukadier, A., Han, M.S., Zhang, X.M., et al. (2015). Hepatic acetyl CoA links adipose tissue inflammation to hepatic insulin resistance and type 2 diabetes. Cell *160*, 745–758.

Perry, R.J., Peng, L., Abulizi, A., Kennedy, L., Cline, G.W., and Shulman, G.I. (2017a). Mechanism for leptin's acute insulin-independent effect to reverse diabetic ketoacidosis. J. Clin. Invest. *127*, 657–669.

Perry, R.J., Peng, L., Cline, G.W., Butrico, G.M., Wang, Y., Zhang, X.M., Rothman, D.L., Petersen, K.F., and Shulman, G.I. (2017b). Non-invasive assessment of hepatic mitochondrial metabolism by positional isotopomer NMR tracer analysis (PINTA). Nat. Commun. *8*, 798.

Perry, R.J., Wang, Y., Cline, G.W., Rabin-Court, A., Song, J.D., Dufour, S., Zhang, X.M., Petersen, K.F., and Shulman, G.I. (2018). Leptin Mediates a Glucose-Fatty Acid Cycle to Maintain Glucose Homeostasis in Starvation. Cell *172*, 234–248.

Porter, C., Herndon, D.N., Chondronikola, M., Chao, T., Annamalai, P., Bhattarai, N., Saraf, M.K., Capek, K.D., Reidy, P.T., Daquinag, A.C., et al. (2016). Human and Mouse Brown Adipose Tissue Mitochondria Have Comparable UCP1 Function. Cell Metab. *24*, 246–255.

Qiu, Y., Nguyen, K.D., Odegaard, J.I., Cui, X., Tian, X., Locksley, R.M., Palmiter, R.D., and Chawla, A. (2014). Eosinophils and type 2 cytokine signaling in macrophages orchestrate development of functional beige fat. Cell *157*, 1292–1308.

Remick, D.G., Bolgos, G., Copeland, S., and Siddiqui, J. (2005). Role of interleukin-6 in mortality from and physiologic response to sepsis. Infect. Immun. *73*, 2751–2757.

Reza, M.M., Subramaniyam, N., Sim, C.M., Ge, X., Sathiakumar, D., McFarlane, C., Sharma, M., and Kambadur, R. (2017). Irisin is a pro-myogenic factor that induces skeletal muscle hypertrophy and rescues denervation-induced atrophy. Nat. Commun. *8*, 1104.

Rothaug, M., Becker-Pauly, C., and Rose-John, S. (2016). The role of interleukin-6 signaling in nervous tissue. Biochim. Biophys. Acta *1863* (6 Pt A), 1218–1227.

Rouget, C., Breuiller-Fouché, M., Mercier, F.J., Leroy, M.J., Loustalot, C., Naline, E., Frydman, R., Croci, T., Morcillo, E.J., Advenier, C., and Bardou, M. (2004). The human near-term myometrial beta 3-adrenoceptor but not the beta 2-adrenoceptor is resistant to desensitisation after sustained agonist stimulation. Br. J. Pharmacol. *141*, 831–841.

Roussou, E., Iacovou, C., Weerakoon, A., and Ahmed, K. (2013). Stress as a trigger of disease flares in SLE. Rheumatol. Int. *33*, 1367–1370.

Russell, G., and Lightman, S. (2019). The human stress response. Nat. Rev. Endocrinol. *15*, 525–534.

Satin, J.R., Linden, W., and Phillips, M.J. (2009). Depression as a predictor of disease progression and mortality in cancer patients: a meta-analysis. Cancer *115*, 5349–5361.

Scheller, J., Chalaris, A., Schmidt-Arras, D., and Rose-John, S. (2011). The pro- and anti-inflammatory properties of the cytokine interleukin-6. Biochim. Biophys. Acta *1813*, 878–888.

Seo, D., Tsou, K.A., Ansell, E.B., Potenza, M.N., and Sinha, R. (2014). Cumulative adversity sensitizes neural response to acute stress: association with health symptoms. Neuropsychopharmacology *39*, 670–680.

Simpson, R., Booth, J., Lawrence, M., Byrne, S., Mair, F., and Mercer, S. (2014). Mindfulness based interventions in multiple sclerosis–a systematic review. BMC Neurol. *14*, 15.

Steensberg, A., Fischer, C.P., Sacchetti, M., Keller, C., Osada, T., Schjerling, P., van Hall, G., Febbraio, M.A., and Pedersen, B.K. (2003). Acute interleukin-6 administration does not impair muscle glucose uptake or whole-body glucose disposal in healthy humans. J. Physiol. *548*, 631–638.

Stumvoll, M., Meyer, C., Perriello, G., Kreider, M., Welle, S., and Gerich, J. (1998). Human kidney and liver gluconeogenesis: evidence for organ substrate selectivity. Am. J. Physiol. *274*, E817–E826.

Timper, K., Denson, J.L., Steculorum, S.M., Heilinger, C., Engström-Ruud, L., Wunderlich, C.M., Rose-John, S., Wunderlich, F.T., and Brüning, J.C. (2017). IL-6 Improves Energy and Glucose Homeostasis in Obesity via Enhanced Central IL-6 trans-Signaling. Cell Rep. *19*, 267–280.

Turner, R.J., and Lloyd, D.A. (1995). Lifetime traumas and mental health: the significance of cumulative adversity. J. Health Soc. Behav. *36*, 360–376.

van Marken Lichtenbelt, W.D., Vanhommerig, J.W., Smulders, N.M., Drossaerts, J.M., Kemerink, G.J., Bouvy, N.D., Schrauwen, P., and Teule, G.J. (2009). Cold-activated brown adipose tissue in healthy men. N. Engl. J. Med. *360*, 1500–1508.

Vida, M., Gavito, A.L., Pavón, F.J., Bautista, D., Serrano, A., Suarez, J., Arrabal, S., Decara, J., Romero-Cuevas, M., de Fonseca, J.R., and Baixeras, E. (2015). Chronic Administration of Recombinant IL-6 Upregulates Lipogenic Enzyme Expression and Aggravates High-Fat-Diet-Induced Steatosis in IL-6-deficient Mice. Dis. Model Mech. *8*, 721–731.

Wallenius, V., Wallenius, K., Ahrén, B., Rudling, M., Carlsten, H., Dickson, S.L., Ohlsson, C., and Jansson, J.O. (2002). Interleukin-6-deficient mice develop mature-onset obesity. Nat. Med. *8*, 75–79.

Wang, A., Huen, S.C., Luan, H.H., Yu, S., Zhang, C., Gallezot, J.D., Booth, C.J., and Medzhitov, R. (2016). Opposing Effects of Fasting Metabolism on Tissue Tolerance in Bacterial and Viral Inflammation. Cell *166*, 1512–1525.

Wang, L.C., Yao, H.W., Chang, C.F., Wang, S.W., Wang, S.M., and Chen, S.H. (2017). Suppression of interleukin-6 increases enterovirus A71 lethality in mice. J. Biomed. Sci. *24*, 94.

Weickert, M.O., and Pfeiffer, A.F. (2006). Signalling mechanisms linking hepatic glucose and lipid metabolism. Diabetologia *49*, 1732–1741.

Weis, S., Carlos, A.R., Moita, M.R., Singh, S., Blankenhaus, B., Cardoso, S., Larsen, R., Rebelo, S., Schauble, S., Del Barrio, L., et al. (2017). Metabolic Adaptation Establishes Disease Tolerance to Sepsis. Cell *169*, 1263–1275.

Wolf, Y., Boura-Halfon, S., Cortese, N., Haimon, Z., Sar Shalom, H., Kuperman, Y., Kalchenko, V., Brandis, A., David, E., Segal-Hayoun, Y., et al. (2017). Brown-adipose-tissue macrophages control tissue innervation and homeostatic energy expenditure. Nat. Immunol. *18*, 665–674.

Wunderlich, F.T., Ströhle, P., Könner, A.C., Gruber, S., Tovar, S., Brönneke, H.S., Juntti-Berggren, L., Li, L.S., van Rooijen, N., Libert, C., et al. (2010). Interleukin-6 signaling in liver-parenchymal cells suppresses hepatic inflammation and improves systemic insulin action. Cell Metab. *12*, 237–249.

Yan, C., Zhang, B.B., Hua, H., Li, B., Zhang, B., Yu, Q., Li, X.Y., Liu, Y., Pan, W., Liu, X.Y., et al. (2015). The Dynamics of Treg/Th17 and the Imbalance of Treg/Th17 in Clonorchis sinensis-Infected Mice. PLoS ONE *10*, e0143217.

Zhang, W., Mottillo, E.P., Zhao, J., Gartung, A., VanHecke, G.C., Lee, J.F., Maddipati, K.R., Xu, H., Ahn, Y.H., Proia, R.L., et al. (2014). Adipocyte lipolysis-stimulated interleukin-6 production requires sphingosine kinase 1 activity. J. Biol. Chem. *289*, 32178–32185.

Zhang, C., Wu, Z., Zhao, G., Wang, F., and Fang, Y. (2016). Identification of IL6 as a susceptibility gene for major depressive disorder. Sci. Rep. *6*, 31264.

Zhang, J.C., Yao, W., Dong, C., Yang, C., Ren, Q., Ma, M., and Hashimoto, K. (2017). Blockade of interleukin-6 receptor in the periphery promotes rapid and sustained antidepressant actions: a possible role of gut-microbiota-brain axis. Transl. Psychiatry *7*, e1138.

Please cite this article in press as: Qing et al., Origin and Function of Stress-Induced IL-6 in Murine Models, Cell (2020), https://doi.org/10.1016/j.cell.2020.05.054

STAR★METHODS

KEY RESOURCES TABLE

REAGENT or RESOURCE	SOURCE	IDENTIFIER
Antibodies		
Anti-mouse IL6	eBioscience	Cat#14-7061-85; RRID: AB_468422
Biotin-conjugated anti-IL6	BD PharMingen	Cat#554402; RRID: AB_395368
HRP-conjugated streptavidin	BD Bioseiences	Cat#554066
Anti-mouse TNFa	eBioscience	Cat#14-7423-85; RRID: AB_468492
Anti-mouse IL-1β	Invitrogen	Cat#14-7012-81; RRID: AB_468396
Biotin-conjugated anti-TNFa	Invitrogen	Cat#13-7349-81; RRID: AB_466952
Biotin-conjugated anti-IL-1β	eBioscience	Cat#13-7112-85; RRID: AB_466925
InVivoMAb anti-mouse IL-6R	Bio X Cell	Cat#BE0047; RRID: AB_1107588
InVivoMAb rat IgG2b isotype control, anti-keyhole limpet hemocyanin	Bio X Cell	Cat#BE0090; RRID: AB_1107780
Biological Samples		
Human plasma	Yale Stress Center	N/A
Chemicals, Peptides, and Recombinant Proteins		
Recombinant mouse IL6	R & D	Cat#406-ML
Recombinant mouse TNFa	R & D	Cat#410-MY
Recombinant mouse IL-1β	R & D	Cat#401-ML-010
NEFA standard solution	Wako Diagnostics	Cat#276-76491
HR series NEFA-HR(2) color reagent A	Wako Diagnostics	Cat#999-34691
HR series NEFA-HR(2) solvent A	Wako Diagnostics	Cat#995-34791
HR series NEFA-HR(2) color reagent B	Wako Diagnostics	Cat#991-34891
HR series NEFA-HR(2) solvent B	Wako Diagnostics	Cat#993-35191
Multi-calibrator lipid	Wako Diagnostics	Cat#464-01601
L-type triglyceride M enzyme color A	Wako Diagnostics	Cat#994-02891
L-type triglyceride M enzyme color B	Wako Diagnostics	Cat#990-02991
Intralipid 20%	Sigma-Aldrich	Cat#1141
Poloxamer 407	Sigma-Aldrich	Cat#16758
Glucose, D-[3-3H]	PerkinElmer	Cat#NET331C250UC
Potassium palmitate (U-13C16)	Cambridge Isotope Laboratories	Cat#CLM-3943-PK
Sodium L-lactate-3-^{13}C solution	Sigma-Aldrich	Cat#490040
6-hydroxydopamine	Sigma-Aldrich	Cat#H4381
Lipopolysaccharides from *Escherichia coli* O55:B5	Sigma-Aldrich	Cat#L2880 Lot#039M4004V
Isoproterenol	Sigma-Aldrich	Cat#1351005
CL316243	Sigma-Aldrich	Cat#C5976
Propranolol	Sigma-Aldrich	Cat#P0884
SR59203A	Cayman Chemical	Cat#21407
Critical Commercial Assays		
Mouse cytokine array/chemokine array 44-plex (MD44)	Eve Technologies	N/A
Human cytokine array/chemokine array 42-plex with IL-18(HD42)	Eve Technologies	N/A
Glycerol assay kit	Sigma-Aldrich	Cat#MAK117-1KT
β-hydroxybutyrate colorimetric assay kit	Cayman Chemical	Cat#700190

(*Continued on next page*)

Please cite this article in press as: Qing et al., Origin and Function of Stress-Induced IL-6 in Murine Models, Cell (2020), https://doi.org/10.1016/j.cell.2020.05.054

Continued

REAGENT or RESOURCE	SOURCE	IDENTIFIER
Corticosterone ELISA kit	Enzo Life Sciences	Cat#ADI-900-097
Mouse insulin ELISA kit	Crystal Chem	Cat#90080
Noradrenaline ELISA kit	Eagle Biosciences	Cat#NOR31-K01
Mouse CTnI	Life Diagnostics	Cat#CTNI-1-US
Alanine transaminase colorimetric activity assay kit	Cayman Chemical	Cat#700260
Experimental Models: Organisms/Strains		
Mouse: C57BL/6J	The Jackson Laboratory	00064
Mouse: Adrb1 ^{tm1Bkk} Adrb2 ^{tm1Bkk}	The Jackson Laboratory	003810
Mouse: B6.129-Ucp1 t^{m1Kz}	The Jackson Laboratory	003124
Mouse: B6;SJL-Il6ra $^{tm1.1Drew}$ / J	The Jackson Laboratory	12944
Mouse: B6. FVB(129)-Tg(Alb-cre)1Dlr / J	The Jackson Laboratory	016832
Mouse: B6. 129-Tg(Adipo q-cre/Esr1*) 1Evdr / J	The Jackson Laboratory	024671
Mouse: Adrenalectomy and sham surgery	The Jackson Laboratory	https://www.jax.org/jax-mice-and-services/find-and-order-jax-mice/surgical-and-preconditioning-services/surgical-service-for-jax-mice
Oligonucleotides		
Primers for mouse Il6 Forward	This paper	TGAACAACGATGATGCACTTG
Primers for mouse Il6 Reverse	This paper	CTGAAGGACTCTGGCTTTGTC
Primers for mouse Il6ra Forward	This paper	AGACCTGGGACCCGAGTTAC
Primers for mouse Il6ra Reverse	This paper	AAGGTCAAGCTCCTCCTTCC
Primers for mouse Fbp1 Forward	This paper	TGGTTCCGATGGACACAAGG
Primers for mouse Fbp1 Reverse	This paper	CCAATGTGACTGGGGATCAAG
Primers for mouse Gck Forward	This paper	TTACACTGGCCTCCTGATGG
Primers for mouse Gck Reverse	This paper	TTTGCAACACTCAGCCAGAC
Primers for mouse Ucp1 Forward	This paper	GTGAACCCGACAACTTCCGAA
Primers for mouse Ucp1 Reverse	This paper	TGCCAGGCAAGCTGAAACTC
Primers for Pck1, G6p, Pcx, Adrb3, Adrb1, Adrb2, Rpl13a, Ikkb, Tnfa, Cxcl1, Mx1, Il12b, Saa3, Prdm16, Il5, Ssa3, Socs3, See Table S1	This paper	N/A
Software and Algorithms		
Prism 8.0	GraphPad Software, Inc.	N/A

RESOURCE AVAILABILITY

Lead Contact

Further information and requests for reagents may be directed to, and will be fulfilled by, the lead contact Andrew Wang (andrew.wang@yale.edu).

Materials Availability

This study did not generate new reagents. Mouse lines for this study are available from the Lead Contact with a completed Materials Transfer Agreement.

Data and Code Availability

This study did not generate any datasets/code amenable for depositing into public repositories.

Please cite this article in press as: Qing et al., Origin and Function of Stress-Induced IL-6 in Murine Models, Cell (2020), https://doi.org/10.1016/j.cell.2020.05.054

EXPERIMENTAL MODEL AND SUBJECT DETAILS

Mice

Male mice with 6-8 weeks of age were used. C57BL/6J, *Adrb1/b2* KO, *Ucp1* KO, *Il6ra* f/f, *Alb*Cre, *Adipo*Cre mice were purchased from Jackson Laboratories and bred at Yale University. *Adrb3* KO mice were a kind gift from Dr. Natasa Petrovic (Stockholm University), *Adrb3* f/f mice were a kind gift from Dr. Jean-Luc Balligand (UC Louvain), the *Ucp1*CreER animal was a kind gift from Dr. Wolfrum Chrsitian (ETH Zurich), the *Il6* f/f was a kind gift from Dr. Juan Pareja (Universitat Autonoma Barecelona) and the *Tlr2/4* KO, and *Myd88/Trif* KO animals were kindly provided by Dr. Ruslan Medzhitov. Adrenalectomy and sham surgery mice were purchased from Jackson Laboratories. All animal experiments were performed according to institutional regulations upon review and approval of Yale University's Institutional Animal Care and Use Committee.

For stress models, all experiments were done during the light period. Acute restraint stress was initiated by retaining a mouse in a ventilated 50ml Falcon tube for four hours. Social isolation was induced by individually housing mouse for three days. Retro-orbital bleeding (50 μL of blood drawn via a glass cuvette VWR #53432-921) was performed four hours before experiments, then blood was collected from the other eye for analysis. In the cage switch model, mice were removed from their home cage and placed in new cage of the same size with dirty bedding of other non-littermate males. Non-disturbed socially-housed littermates were applied as the controls. For anesthesia studies, ketamine/xylazine was injected intraperitoneally or animals were placed in isoflurane chambers. Verification of anesthesia was confirmed by lack of activity after toe pinching. Chemically sympathectomized with 6-hydroxydopamine (6-OHDA, sigma) was applied through intraperitoneal injection 24 hours before acute stress at a dosage of 10 mg/kg. For manipulation of ambient temperature, mice were either housed at thermoneutral (32°C) cabinets for two weeks, or placed in the cold (4°C) for three hours, or housed at standard housing (22°C).

For flux and metabolite measurements, mice underwent surgery under isoflurane anesthesia to place a catheter in the left jugular vein. Animals were individually housed with unrestricted access to food and water and were treated again with IL-6Ra antibody or isotype control the night before a 120 min tracer infusion, performed after two hours of acclimation to a 1.25 inch diameter plastic restrainer (IBI Scientific) in which the mouse's tail was drawn through the restraint and tethered with tape, while an adjustable nose cone permitted the mouse several centimeters of forward movement. At the conclusion of the tracer infusion, mice were euthanized via IV pentobarbital and liver and kidney were obtained and freeze-clamped in liquid N_2 within 30 s of euthanasia.

For LPS endotoxemia, mice were injected intraperitoneally with LPS derived from *Escherichia coli* 055:B5 (Sigma-Aldrich) diluted in PBS. Dosing varies dramatically from lot to lot. New lots are tested for LD50. In these studies, lethal doses are between 15 and 20 mg/kg. For experiments with antibody blockade, anti-IL-6Ra or the isotype antibody (BE0047 and BE0090 respectively, Bio X Cell, 8 mg/kg) diluted in PBS was injected intravenously one night before experiment through retro-orbital injection. For experiments utilizing recombinant IL-6, recombinant mouse IL-6 (406-ML-025/CF, R&D) or PBS control was intravenously injected one hour before experiment at a dose of 5ng/100 μl/mouse through the retro-orbital plexus. For experiments utilizing adrenergic agonists, ADRB1/2 agonist (Isoproterenol, 1351005, Sigma-Aldrich, 1mg/kg), ADRB3 agonist (CL316243, Sigma-Aldrich, 1mg/kg) were injected intraperitoneally two hours prior to blood and tissue harvesting. For adrenergic antagonists, propranolol (5 mg/kg, P0884, Sigma-Aldrich) and ADRB3 antagonist (SR59203A, 21407, Cayman Chemical, 5mg/kg) were applied once every two hours during four-hour-exposure of acute stresses, blood were collected at indicated time point, and lethal dose of LPS was administered two hours after last injection of ADRB3 antagonist.

Vital signs, including blood oxygen saturation, breath rate, and heart rate post LPS injection were monitored via pulse oximetry using the MouseOx Plus (Starr Life Sciences Corp.). Core body temperature was measured by rectal probe thermometry (Physitemp TH-5 Thermalert).

Human Subjects

A community sample of individuals signed written informed consent for research approved by the Yale Institutional Review Board and was carefully assessed for high and low stress using a structured cumulative stress and adversity interview that assessed recent and past life events (Cumulative Adversity Interview (CAI)) (Ansell et al., 2012; Seo et al., 2014; Turner and Lloyd, 1995). The high and low groups were group matched on age, gender, education and body mass index (BMI). All subjects participated in two standardized experiment sessions on consecutive days conducted between 2:00 and 4:00 pm in the afternoon. Baseline blood draws were drawn at 2 pm after a one-hour habituation period and two additional draws were conducted within 15 minutes. Change from baseline values were computed to assess baseline adjusted values and reduce variability across subjects.

METHOD DETAILS

Quantification of Plasma Cytokines

Undiluted plasma from stressed mice were screened by Eve Technologies using mouse cytokine arrays, the raw data including standard results were presented in Figure S7A. Except for the results in Figures 1B and S1E from samples analyzed by Eve Technologies, other analyses were conducted in our laboratory. Plasma concentrations of IL-6 were assayed by sandwich ELISA (Luan et al., 2019; Wang et al., 2016). Anti-mouse IL-6 capture antibody (14-7061-85, eBioscience) was diluted (1:1000) in coating buffer (NaHPO4 PH 9) then incubated in enhanced protein-binding ELISA-grade plate (490012-252, VWR) overnight at 4°C. On the next day plates were

Please cite this article in press as: Qing et al., Origin and Function of Stress-Induced IL-6 in Murine Models, Cell (2020), https://doi.org/10.1016/j.cell.2020.05.054

blocked using PBS buffer with 10% FBS for one hour at room temperature. Afterward, the standards and plasma from stressed mice were incubated in the plate overnight at 4°C. The highest concentration of recombinant IL-6 standard (406-ML, R&D) was 10ng/ml followed by serial two-fold dilutions to create a standard curve, and plasma were diluted 1:5 (20ul plasma in 80ul blocking buffer per well). On the third day, biotin-conjugated anti-IL-6 detection antibodies (554402, BD PharMingen) was diluted (1:500) and incubated in the plate for one hour at room temperature, followed with another incubation of diluted (1:1000) HRP-conjugated streptavidin (554066, BD Biosciences) for half an hour at room temperature. Then plates were incubated in the dark at room temperature with TMB substrate reagent (555214, BD Biosciences) and the color was checked every five minutes. Then plates were read at 450nm instantly after stop solution (3M H_2SO_4) was added. Between each step, five to seven times of washing were normally applied. The raw data, results of standard curve and representative plate with color developed with TMB were displayed in Figures S7B–S7E. Plasma concentrations of TNFα and IL-1β were assayed by the same sandwich ELISA method. Recombinant TNFα (410-MY, R&D) and IL-1β (401-ML-010, R&D) were utilized as standards with the highest concentration at 10ng/ml and 1ng/ml respectively. Capture antibodies were anti-TNFα (14-7423-85, eBioscience) and anti-IL-1β (14-7012-81, Invitrogen). Detection antibodies conjugated with biotin were anti-mouse TNFα (13-7349-81, Invitrogen) and anti-mouse IL-1β (13-7112-85, eBioscience). HRP-conjugated streptavidin, TMB substrate reagent, and stop solution were the same with those in ELISA assay for IL-6 measurement.

Quantification of Plasma Metabolites, Hormones, and Organ Injury Markers

Glycemia was measured by whole blood collection via the retro-orbital plexus and assessed using a glucometer (OneTouch), or, during the flux studies in IL-6Ra treated mice, in blood collected from the tail vein using the YSI Glucose Analyzer. Plasma was separated using lithium heparin-coated microcentrifuge tubes (BD Diagnostics). Plasma L-type triglycerides (TG) and nonesterified fatty acids were measured using the kits according to manufacturer's instructions (Wako Diagnostics). Plasma Glycerol and β-hydroxybutyrate were measured using the kits per manufacturer's instructions (Sigma Aldrich and Cayman Chemical, respectively). Plasma amino acid concentrations were measured by gas chromatography-mass spectrometry (GC-MS) as described previously (Perry et al., 2018). Plasma levels of corticosterone (Enzo Life Sciences), insulin (Crystal Chem), and noradrenaline (Eagle Biosciences) were measured using kits according to the manufacturer's protocols. Cardiac Troponin-I (CTNI) concentration and Alanine Aminotransferase (ALT) activity in the blood were measured by kits per manufacturers' instructions (Life Diagnostics and Cayman Chemical, respectively). Plasma creatinine were assayed using HPLC by the George M. O'Brien Kidney Center at Yale.

Surgical Removal of Brown Adipose Tissue

Surgical removal of brown adipose tissue (BAT) was applied to seven weeks old male mice. A 1.5 cm incision was made to expose the intrascapular fat pads following intraperitoneal injection of ketamine/xylazine. Two lobes of darkly colored BAT were completely removed with little bleeding. Sham-operated mice were anesthetized and incisions were made into the muscles without tissue excision. Heat mats were applied to keep all animals warm during and after surgery until consciousness was fully recovered. Then mice were kept in room temperature, and IL-6 secretion post retro-orbital bleeding was analyzed in these mice two days after surgery.

Metabolic Tolerance Tests

For oral GTT, D-Glucose (G8270, Sigma-Aldrich) or water gavage was performed; blood was collected afterward through retro-orbital plexus at indicated time point for glucose and IL-6 analysis. For intraperitoneal GTT, D-glucose was given through intraperitoneal injection at the dose of 2g/kg. CBG was analyzed using a glucometer (OneTouch) at indicated time points. For insulin tolerance tests, insulin (Novolin R) was administrated at 2 IU/kg through intraperitoneal injection. For pyruvate tolerance tests, pyruvate (Sigma-Aldrich) was applied at 2g/kg by intraperitoneal injection. CBG was analyzed at indicated time points. For lipid tolerance tests, intralipid 20% (1141, Sigma-Aldrich) was intraperitoneally injected at a volume of 200 μL per mouse. Plasma level of TG was analyzed at 0, 1, 2, 3, and 4 hours after intralipid administration. For hepatic triglyceride production, poloxamer 407 (16758, Sigma-Aldrich) was dissolved in PBS and then intraperitoneally injected at 1g/kg. Plasma level of TG was analyzed at 0, 1, 2, 3, and 4 hours after poloxamer injection. Mice were fasted overnight before the hepatic TG production assay and assessment of glucose and palmitate turnover; for all other tolerance tests, stressed or unstressed mice were fasted for four hours before testing. Capillary blood glucose (CBG) was analyzed using a glucometer (OneTouch) at indicated time points.

Endogenous Glucose Production and Palmitate Turnover

After anti-IL-6Ra treatment, endogenous glucose production and palmitate turnover from C57BL/6J mice were measured as precious described (Perry et al., 2017a, 2017b). In brief, IL-6Ra inhibitor or vehicle control was injected through orbital venous plexus respectively before catheter placement and tracer infusions. Mice were infused with [3-^{3}H] glucose (10 μCi/min, PerkinElmer), [U-$^{13}C_{16}$] potassium palmitate (2.5 μmol/kg/min, Cambridge Isotopes), and [3-^{13}C] sodium lactate (40 μmol/kg/min, Sigma) continuously for a total of two hours following a 5 min 3X prime. Palmitate turnover was determined by gas chromatography-mass spectrometry (GC-MS) (Perry et al., 2017a). Plasma specific activity was measured using a scintillation counter and compared to tracer specific activity to measure whole-body endogenous glucose production, which can be attributed entirely to gluconeogenesis in a 16 hr fasted, glycogen-depleted mouse. Based on equations previously described (Perry et al., 2017b), and after verifying minimal (atom percent enrichment < 1%, as compared to glucose 15%–20%) renal and hepatic bicarbonate enrichment, we measured the

whole-body ratio of pyruvate carboxylase flux (i.e., gluconeogenesis from pyruvate) to total gluconeogenesis by mass isotopomer distribution analysis (MIDA):

$$GNG\ from\ pyruvate = \frac{[C_2\ 13]glucose}{XFE^2} \quad (1)$$

where XFE represents the fractional triose enrichment and is calculated as

$$XFE = \frac{1}{1 + \frac{[C_1\ 13]glucose}{2*[C_2\ 13]glucose}}. \quad (2)$$

In these calculations, we corrected for any [$^{13}C_2$] glucose synthesized from [$^{13}C_2$] trioses – as opposed to the condensation of two [$^{13}C_1$] trioses – by GC-MS measurement of the enrichment in the glucose C4C5C6 fragment, according to the equation

$$Corrected\ [C_2 13]glucose = Measured\ [C_2\ 13]glucose - 2 * [C4C5C6 - C_2\ 13]glucose \quad (3)$$

This ratio was measured in plasma (representing whole-body gluconeogenesis from pyruvate), liver, and renal cortex. By comparing the whole-body gluconeogenesis from pyruvate (GNG from pyruvate$_T$) to that measured in liver (GNG from pyruvate$_L$) and kidney (GNG from pyruvate$_K$), we were able to measure the fractional contribution of the kidney to whole-body gluconeogenesis (GNG_K/GNG):

$$\left(\frac{GNG_K}{GNG}\right) = 1 - \frac{GNG\ from\ pyruvate_T - GNG\ from\ pyruvate_K}{GNG\ from\ pyruvate_L - GNG\ from\ pyruvate_K} \quad (4)$$

Absolute rates of gluconeogenesis from kidney could then be calculated by multiplying the measured endogenous glucose production by (GNG_K/GNG) (Equation 4), and gluconeogenesis from liver was calculated as the difference between total endogenous glucose production and gluconeogenesis from kidney. The rate of gluconeogenesis from liver and kidney was then multiplied by the fractional contribution of pyruvate to gluconeogenesis in those tissues to calculate the contribution of pyruvate to gluconeogenesis in each tissue.

qRT-PCR

Tissues were homogenized in 1ml RNA-Bee (Tel-Test, Inc) using a FastPrep-24 5G homogenizer (MP Biomedicals). RNA was purified using QIAGEN RNeasy columns according to the manufacturer's instructions. cDNA was generated with reverse transcriptase (Clontech) using oligo-dT6 primers (Sigma-Aldrich). qRT-PCR was performed on a CFX96 Real-Time System (Bio-Rad) using PerfeCTa SYBR Green SuperMix (Quanta Biosciences). Relative expression units were calculated as transcript levels of target genes relative to *Rpl13a*. Primers used for qRT-PCR are listed in Table S1.

Stromal Vascular Fraction Isolation

Stromal vascular fraction (SVF) were isolated by density separation as previously reported (Aune et al., 2013). Briefly, interscapular BAT depots were minced and digested in collagenase at 37°C for 1 hour with constant agitation. Then after filtering through 70 μM cell strainer, the cell suspensions were centrifuged at 500 g for 5 min. The pellet was the SVF fraction.

Metabolic Cage

Energy expenditure after acute stress was measured by indirect calorimetry using metabolic cages (Promethion, Sable Systems International). A 2-day period of acclimation was followed by 2 days of steady-state recording prior to experimentation. Afterward, C57BL/6J mice were given IL-6Ra antibody or isotype control through intravenous injection; the next morning, both groups were subjected to retro-orbital bleeding stress.

Ambulatory Blood Pressure Measurements

A blood pressure transducer (TA11-PA-C10, commercially available through Data Sciences International) was surgically implanted under isoflurane anesthesia (1%–3% in oxygen) into the carotid artery of mice using sterile surgical technique. Meloxicam was provided for 48 hours for post-operative analgesia and the skin was closed with surgical staples. Mice were allowed to recover for 7 days. Afterward, surgical staples were removed, and the mice were transferred to a fresh cage and singly housed for data collection. There they were allowed to acclimate for several days prior to initiation of study. A 10 s segment was collected every minute for the duration of the experiment. Every dot in the figure reflects the averaged value over one hour reading period.

Behavioral Tests

The spontaneous exploratory behavior of mice following acute stress was analyzed three hours post retro-orbital bleeding using the light-dark paradigm. All experiments were performed between 11AM and 12 noon in male mice 6-8 weeks of age. Non-stressed mice were habituated to the environment three hours prior to being placed in the light/dark box; three days later, the same mice were

Please cite this article in press as: Qing et al., Origin and Function of Stress-Induced IL-6 in Murine Models, Cell (2020), https://doi.org/10.1016/j.cell.2020.05.054

transferred to the testing room one night before the experiment for acclimatization, then retro-orbital bleeding or tube restraint was performed three hours before light/dark box test. The light/dark box consisted of two of the same-sized chambers (18x10x13 cm), a dark chamber and an equal size light chamber connected by a small central aperture (3.8x3.8x3.8cm). Urine and feces were removed and the box was cleaned after each trial. Mice were initially placed in the corner of the light chamber facing away from the opening and monitored for 6 minutes after the first entry into the dark section. The latency time for the first passage from the light section to the dark one, transitions between the two compartments, and the amount of time spent in the dark were recorded (Mineur et al., 2007).

Immunohistochemistry

Mice were euthanized and perfused with PBS or fixative. Brown adipose tissues were immersion-fixed in 10% neutral buffered formalin. Then tissues were trimmed, processed, embedded, and sectioned and stained for IL-6.

QUANTIFICATION AND STATISTICAL ANALYSIS

Statistical analyses were performed using Prism 8.0 (GraphPad Software, Inc.). For parameters obtained from metabolic cage, the area under a curve was calculated followed by Student's t test. Student's t test was used for two groups comparison. More than two groups were compared using one-way analysis of variance (ANOVA) followed by Tukey test. Samples at different time points from multiple groups were analyzed using two-way ANOVA followed by Tukey test. The log-rank Mantel-Cox test was used to compare Kaplan Meier curves. A p value less than 0.05 was considered statistically significant. Data are presented as the mean ± SEM. * $p < 0.05$, ** $p < 0.01$, *** $p < 0.001$, **** $p < 0.0001$

Supplemental Figures

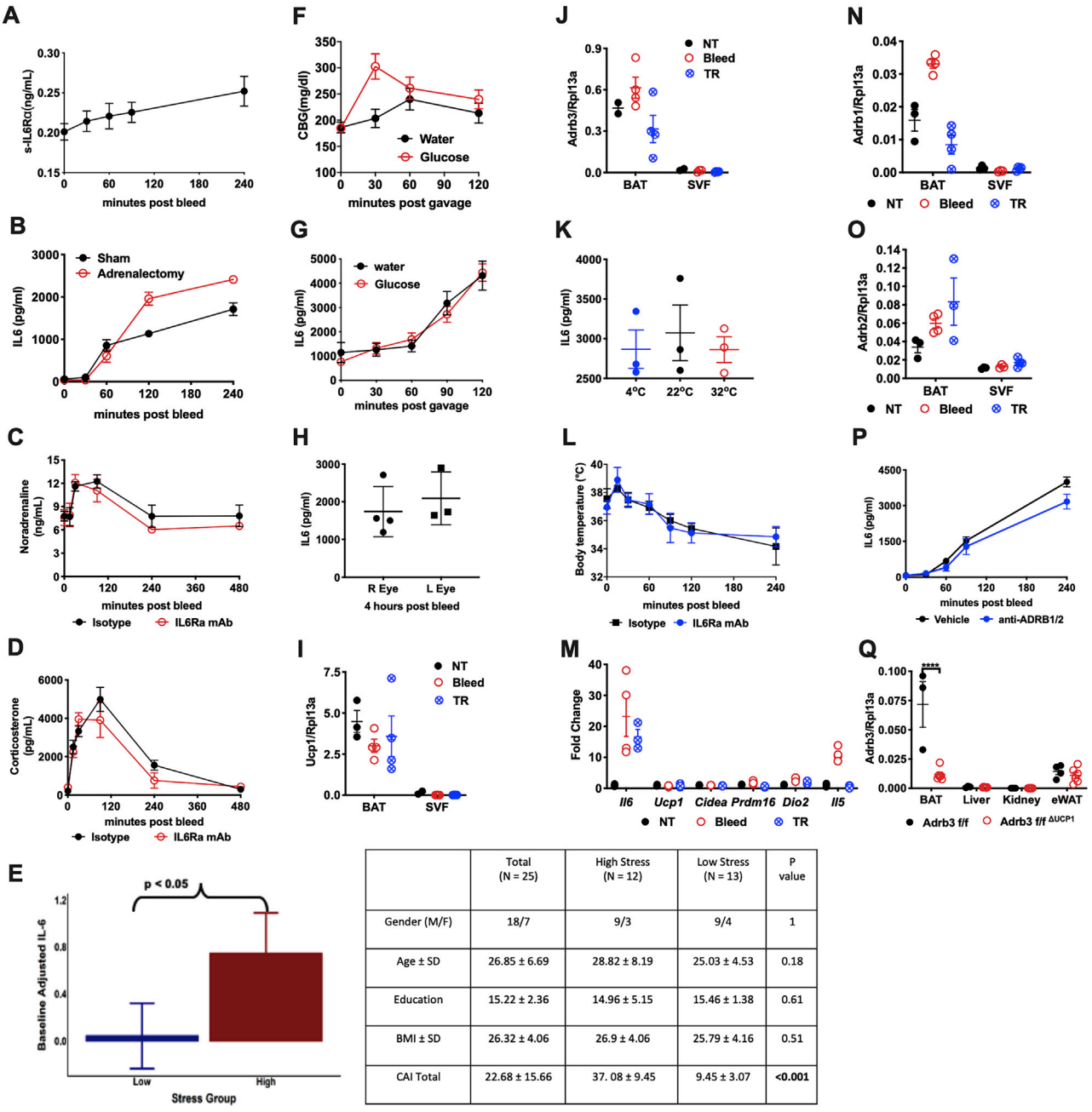

	Total (N = 25)	High Stress (N = 12)	Low Stress (N = 13)	P value
Gender (M/F)	18/7	9/3	9/4	1
Age ± SD	26.85 ± 6.69	28.82 ± 8.19	25.03 ± 4.53	0.18
Education	15.22 ± 2.36	14.96 ± 5.15	15.46 ± 1.38	0.61
BMI ± SD	26.32 ± 4.06	26.9 ± 4.06	25.79 ± 4.16	0.51
CAI Total	22.68 ± 15.66	37. 08 ± 9.45	9.45 ± 3.07	**<0.001**

Figure S1. ADRB3 Mediates Brown Adipocyte-Derived IL-6 in Response to Acute Stress, Related to Figures 1, 2, and 3

(A) Plasma concentrations of soluble IL-6 receptor (s-IL6Ra) from bled mice (n = 5 per group).

(B) Plasma IL-6 levels post-bleeding in mice with bilateral adrenalectomy or sham (n = 5 per group).

(C) Plasma noradrenaline and (D) corticosterone in mice pretreated with IL-6Ra antibody or isotype control (n = 5 per time point per group).

(E) Relative level of circulating IL-6 from human with high or low stress history (n = 12 for high stress history, n = 13 for low stress history).

(F) Capillary blood glucose (CBG) and (G) plasma IL-6 from WT mice after glucose or water gavage. Mice were bled then fasted for four hours before gavage (n = 5 per group).

(H) Plasma IL-6 levels in blood collected from the indicated site of mouse eyes four hours post bleeding (n = 5 per group).

(legend continued on next page)

(I) qPCR analyses of *Ucp1* and (J) *Adrb3* in brown adipocyte tissue (BAT) or the stromal vascular fraction (SVF) from mice stressed with the indicated conditions (n = 5 per group).
(K) Plasma concentration of IL-6 four hours post bleeding from mice subjected to the indicated ambient temperature (n = 3 per group, representative of 2 experiments).
(L) Body temperature after bleeding stress in the presence of IL-6Ra antibody or isotype control (n = 5 per group).
(M) Transcriptional analyses of cold-sensitive genes and *Il5* in BAT (n = 3-4 per group). Results are expressed as fold change relative to non-stressed control (NT).
(N-O) Transcriptional expression of beta-adrenergic receptors *Adrb1* and *Adrb2* in BAT or SVF from BAT of stressed mice (n = 3-4 per group).
(P) Plasma IL-6 levels at indicated time points post bleeding from mice pre-treated with an ADRB1/2 antagonist propranolol (anti-ADRB1/2) or PBS (n = 5 per group).
(Q) Expression of *Adrb3* in the indicated tissues from mice with conditional *Ucp1*-medidated deletion of *Adrb3* (n = 4 per group). *p < 0.05, **p < 0.01, ***p < 0.001, ****p < 0.0001

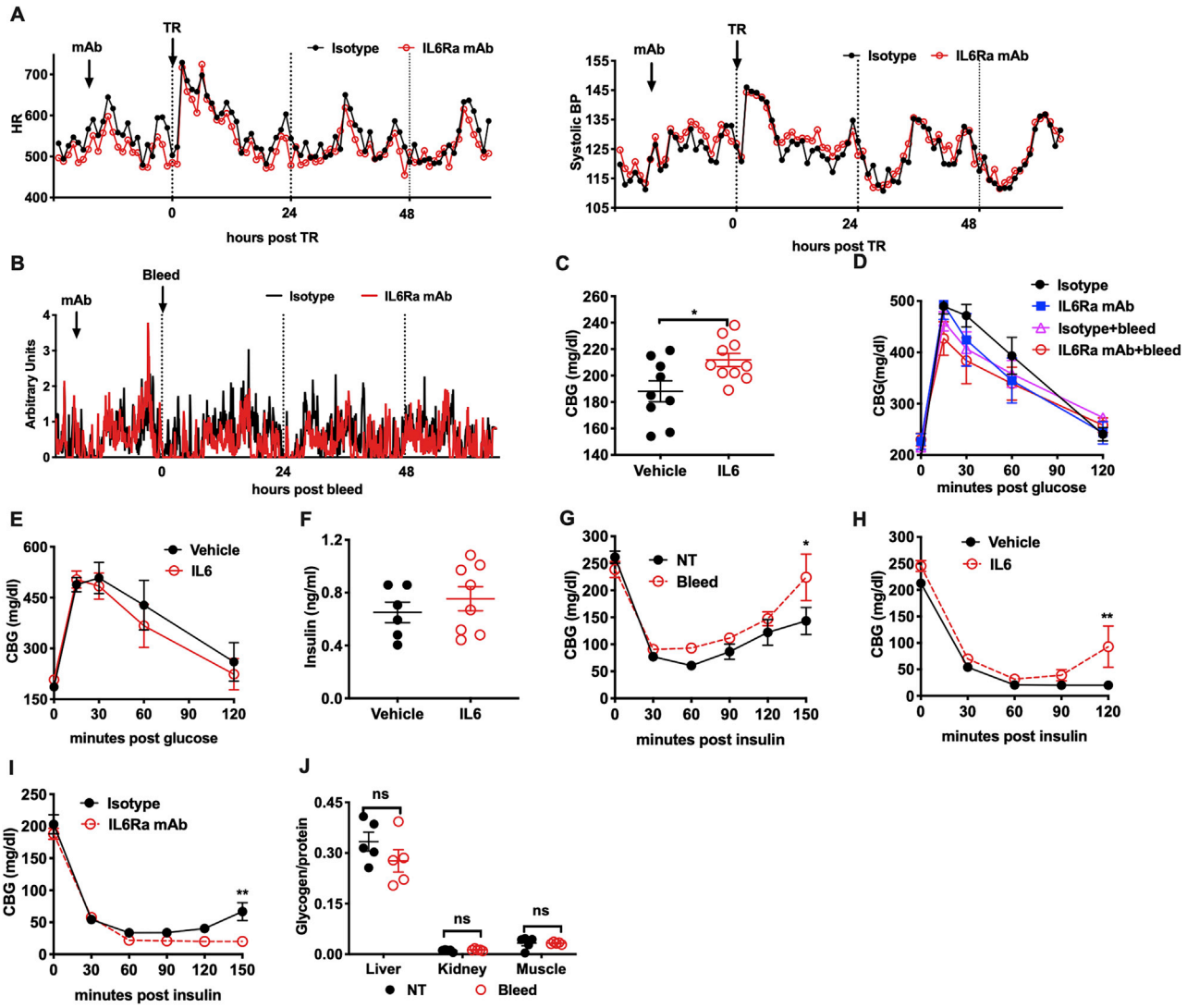

Figure S2. IL-6 Is Necessary for Promoting Stress-Hyperglycemia, Related to Figure 4

(A) Continuous heart (HR) and blood pressure (BP) tracings in mice treated with IL-6Ra mAb or isotype control followed by tube restraint (TR) (n = 4 per group).

(B) Activity of mice treated with IL-6Ra antibody of isotype control followed by retro-orbital bleeding (n = 4 per group, representative of 2 experiments).

(C) Capillary blood glucose (CBG) one hour after injection of stress-dosed IL-6 (n = 10 per group).

(D) Glucose tolerance test (GTT) performed four hours post bleeding from mice pretreated with IL-6Ra antibody or isotype control (n = 5 per group, representative of 3 experiments).

(E) GTT performed one hour after injection with IL-6 or vehicle control (n = 5 per group).

(F) Plasma insulin levels one hour after injection with IL-6 or vehicle control (n = 6 for vehicle, n = 8 for IL-6).

(G) Insulin tolerance test performed in animals four hours after a single retro-orbital bleeding (n = 5 per group, representative of 2 experiments). NT, no treatment.

(H) Insulin tolerance test performed one hour after a stress-dose IL-6 injection (n = 6 per group).

(I) Insulin tolerance test performed in mice pretreated with IL-6Ra antibody or isotype control (n = 5 per group)

(J) Glycogen content in the indicated tissues of mice 3 hours post bleeding (muscle is gastrocnemius, n = 5 per group). *p < 0.05, **p < 0.01, ***p < 0.001, ****p < 0.0001

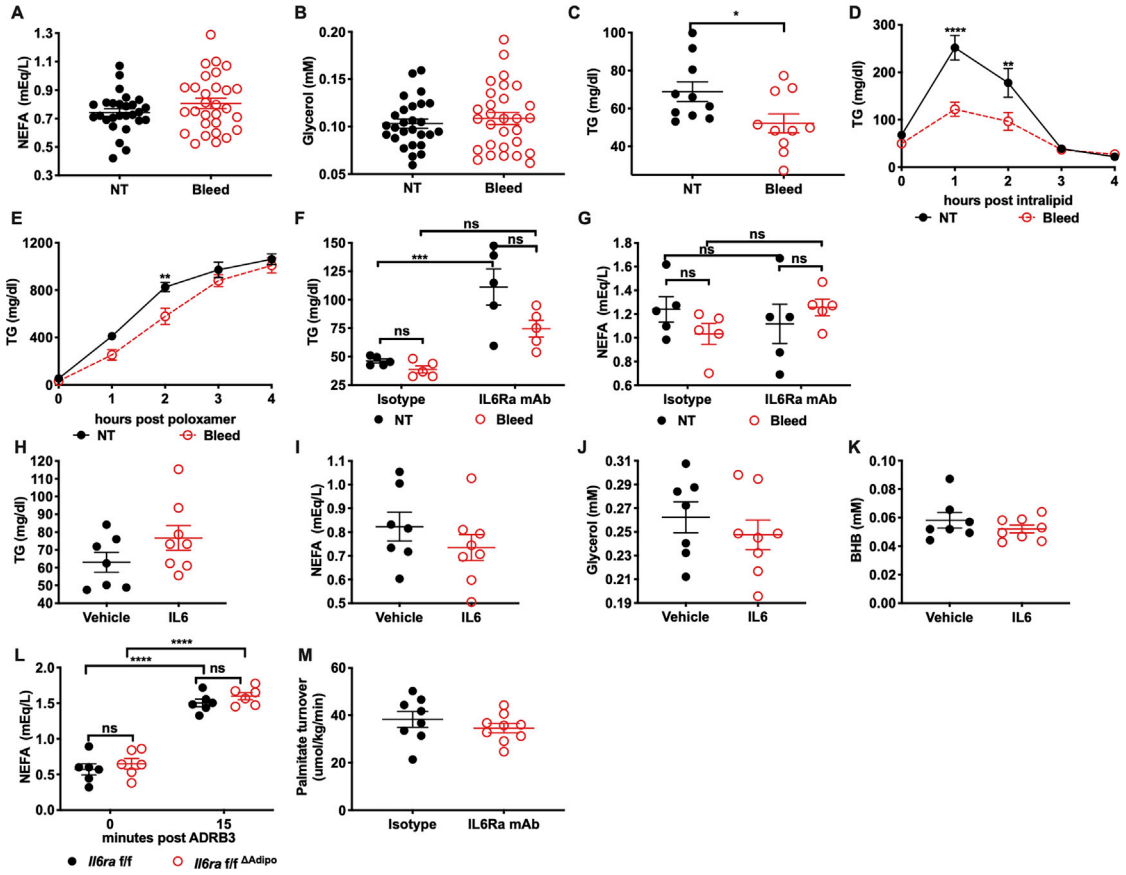

Figure S3. Lipid Metabolism in Response to Acute Stress or External IL-6, Related to Figure 4

(A-C) (A) Plasma levels of non-esterified fatty acid (NEFA), (B) glycerol, and (C) triglycerides (TG) four hours post bleeding (n = 28 for NT, n = 29 for Bleed. Pooled from 3 experiments).

(D) Intralipid tolerance test performed four hours post bleeding (n = 5 per group).

(E) Hepatic triglyceride secretion at indicted time points post poloxamer injection from bled mice or controls (NT) (n = 5 per group).

(F-G) (F) Plasma levels of TG, (G) NEFA assessed four hours post bleeding in mice pretreated with IL-6Ra antibody or isotype control (n = 5 per group).

(H-K) (H) Plasma levels of TG, (I) NEFA, (J) Glycerol, (K) β-Hydroxybutyrate (BHB) one hour after IL-6 injection (n = 5 per group).

(L) *In vivo* lipolysis assay performed using ADRB3 agonist CL316,243 in mice with conditional *Il6ra* deletion in the adipose tissue (*Il6ra*f/f$^{\Delta Adipo}$) or littermate controls (*Il6ra*f/f) (n = 6 per group).

(M) Palmitate turnover assessed in mice treated with IL-6Ra antibody or isotype control (n = 8 per group). *p < 0.05, **p < 0.01, ***p < 0.001, ****p < 0.0001

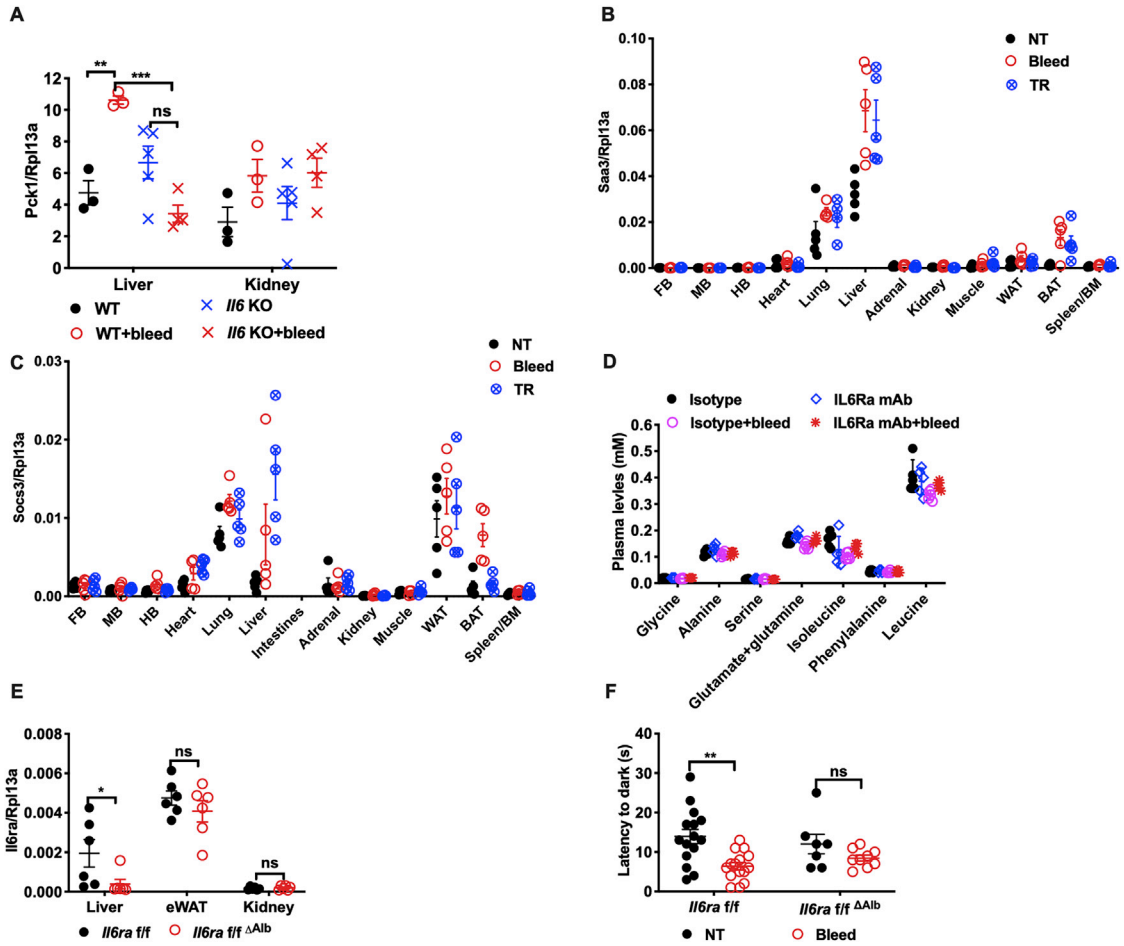

Figure S4. IL-6 Mediates Stress Hyperglycemia through Hepatocyte Reprogramming, Related to Figure 5

(A) *Pck1* mRNA measured at four hours post bleeding from the liver and kidney of *Il6* KO or WT mice (n = 5 per group)

(B) Expression of *Saa3* and (C) *Socs3* in the indicated tissues from stressed mice (n = 5 per group).

(D) Plasma level of amino acids four hours post bleeding in mice pretreated with IL-6Ra antibody or isotype control (n = 5 per group).

(E) *Il6ra* expression in the indicated tissue from mice with liver-specific deletion of *Il6ra* (*Il6ra*f/f$^{\Delta Alb}$) or littermate controls (*Il6ra*f/f) (n = 6 per group).

(F) Latency to dark in mice with liver-specific *Il6ra* deletion (n = 15 for *Il6ra*f/f, n = 9 for *Il6ra*f/f$^{\Delta Alb}$, representative of 3 experiments). *p < 0.05, **p < 0.01, ***p < 0.001, ****p < 0.0001

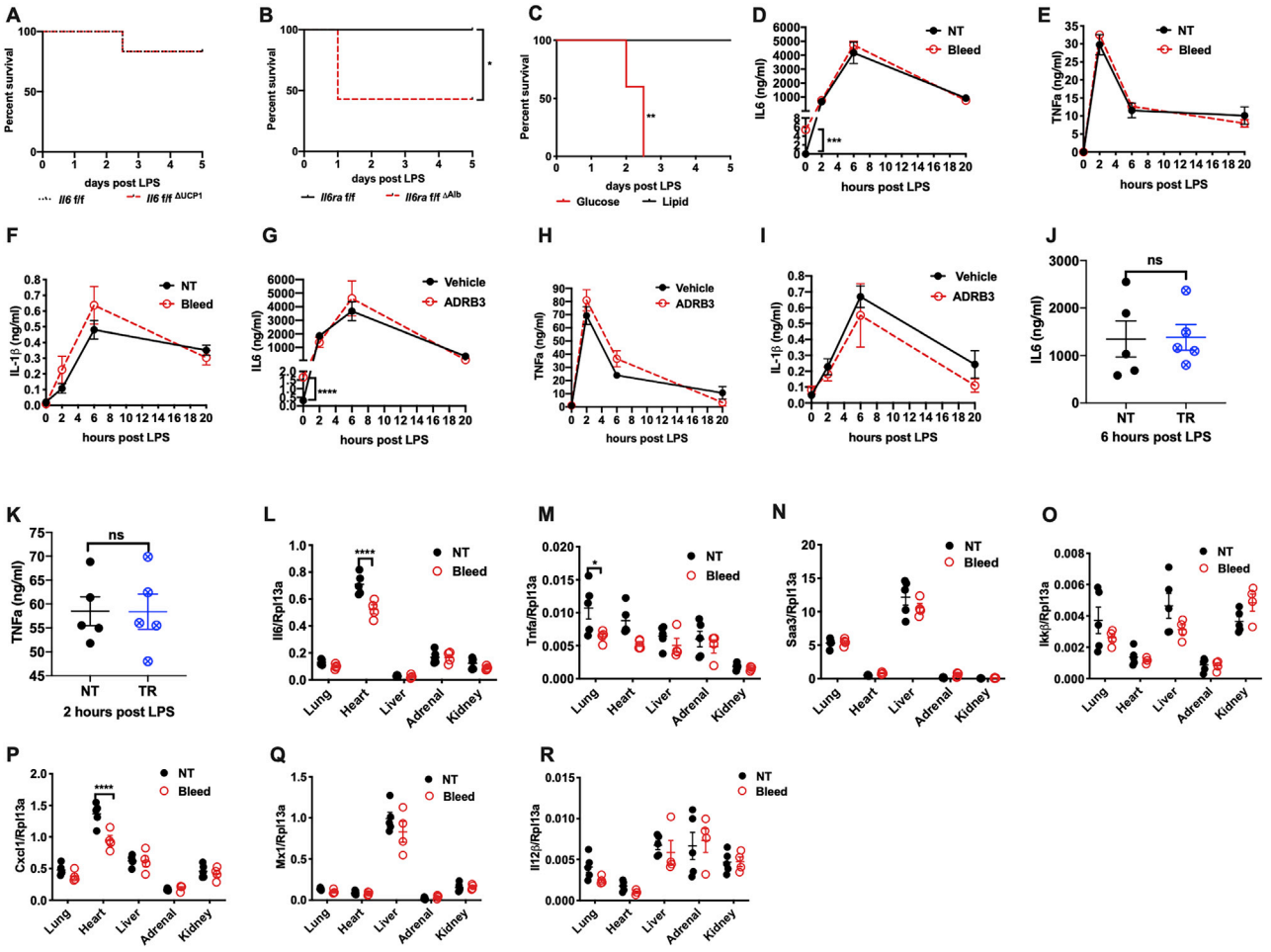

Figure S5. Inflammatory Responses to a Lethal Endotoxemia Are Not Affected by the Pre-exposure of Acute Stress, Related to Figure 6

(A) Survival rate of mice with brown adipose tissue specific deletion of *Il6* (*Il6*/f/f$^{\Delta UCP1}$) comparing with littermate controls (*Il6*f/f) (n = 6 per group, representative of 2 experiments).

(B) Survival rate of mice with liver specific deletion of *Il6ra* (*Il6ra*f/f$^{\Delta Alb}$) comparing with littermate controls (*Il6ra*f/f) (n = 6 per group, representative of 3 experiments).

(C) Survival of animals pre-treated with glucose or an isocaloric isovolumetric dose of intralipid followed by LPS injection (n = 5 per group).

(D) Plasma IL-6, (E) TNFα, and (F) IL-1β levels sampled 0, 2, 6, and 20 hours after LPS challenge in bled mice or non-bled controls (n = 5 per group, representative of 2 experiments).

(G) Plasma IL-6, (H) TNFα, and (I) IL-1β levels sampled 0, 2, 6, and 20 hours after LPS challenge in mice pre-challenged with ADRB3 agonist or vehicle control (n = 5 per group).

(J) The peak levels of circulating IL-6 and (K) TNFα during LPS-mediated endotoxemia from mice pre-exposed to tube restraint (TR) or controls (NT) (n = 5 per group).

(L-R) Expression of inflammatory transcripts in the indicated tissues from LPS-treated mice pre-exposed to bleeding stress. Tissues were harvested three hours after LPS challenge (n = 5 per group). *p < 0.05, **p < 0.01, ***p < 0.001, ****p < 0.0001

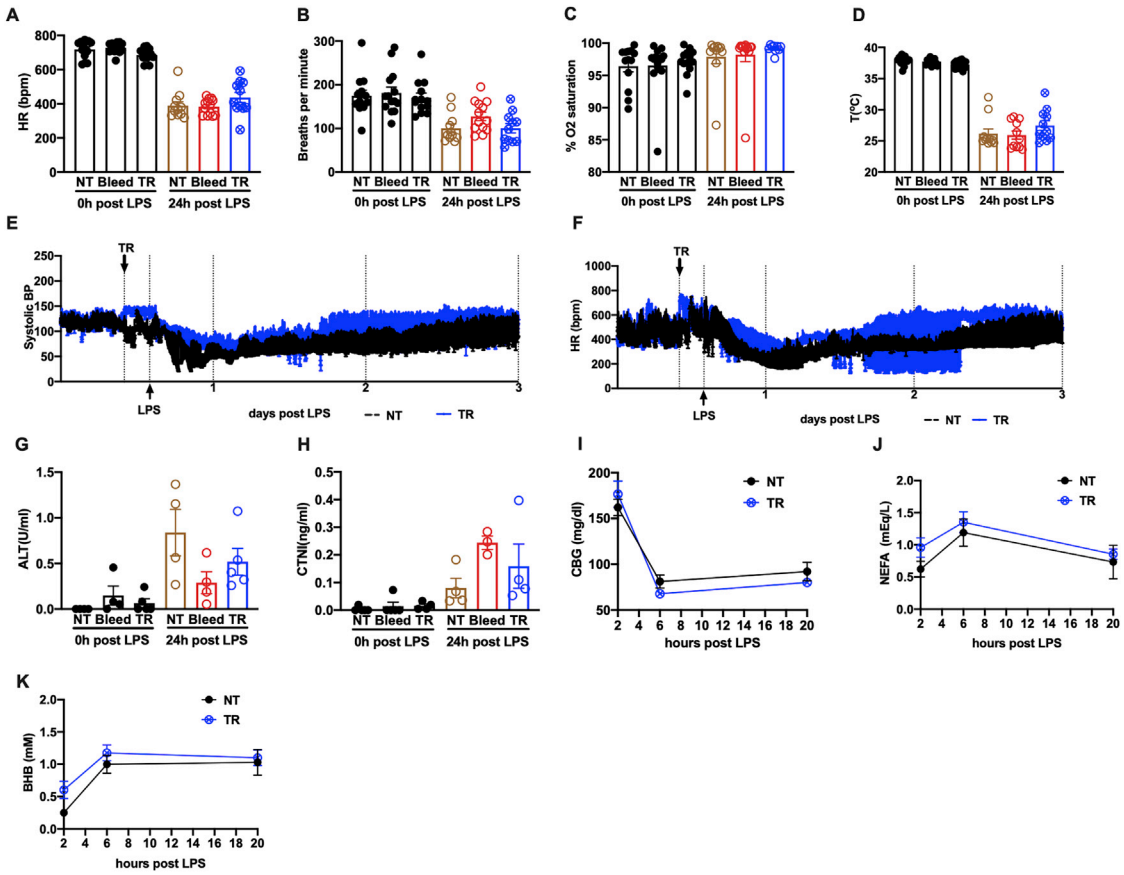

Figure S6. BAT-Derived IL-6 from Acute Stress Decreases Host Tolerance to Inflammatory Damage, Related to Figure 6

(A-D) Vital signs before and 24 hours post LPS challenge from mice pre-exposed to acute stress. NT, no treatment. TR, tube restraint. HR, heart rate.

(E) Continuous systolic blood pressure (BP) and (F) heart rate (HR) tracings in mice with tube restraint and the subsequent LPS challenge. NT, no treatment. TR, tube restraint.

(G) Circulating alanine aminotransferase (ALT) and (H) cardiac troponin I (CTNI) levels 0 or 24 hours post LPS injection from mice pre-exposed to bleeding or restraint stress (n = 5 per group). NT, no treatment. TR, tube restraint.

(I) Capillary blood glucose (CBG) levels post LPS injection at indicated time points from mice pre-exposed to restraint stress (n = 5 per group, representative of 2 experiments). NT, no treatment. TR, tube restraint.

(J) Plasma non-esterified fatty acid (NEFA) levels post LPS injection at indicated time points from mice pre-exposed to restraint stress (n = 5 per group, representative of 2 experiments).

(K) Plasma β-hydroxy-butyrate (BHB) levels post LPS injection at indicated time points from mice pre-exposed to restraint stress (n = 5 per group, representative of 2 experiments).

A

Units: pg/mL

		IL-6 (34)	IL-6 (34)	IL-6 (34)
Description	Dilution	FI	Obs Conc	Exp Conc
Standard 1	1	19	0.64	0.64
Standard 2	1	44	3.20	3.20
Standard 3	1	153	16.00	16.00
Standard 4	1	703	80.00	80.00
Standard 5	1	3575	400.00	400.00
Standard 6	1	11319	2000.00	2000.00
Standard 7	1	22744	10000.00	10000.00
1	1	29	1.68	
2	1	24	1.11	
3	1	22	0.95	
4	1	65	5.54	
5	1	31	1.89	
6	1	3087	343.69	
7	1	3313	369.45	
8	1	8509	1182.86	
9	1	1472	165.31	
10	1	2509	279.06	
11	1	10810	1822.81	
12	1	13560	2865.84	
13	1	11176	1949.45	
14	1	8101	1095.29	
15	1	12602	2478.35	
16	1	47	3.57	
17	1	333	37.54	
18	1	325	36.60	
19	1	317	35.66	
20	1	745	84.70	

D

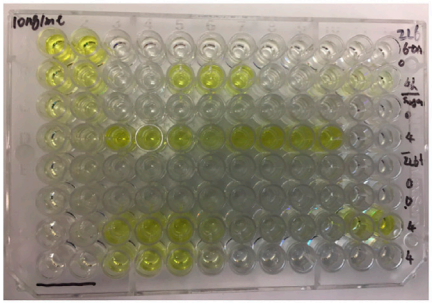

E

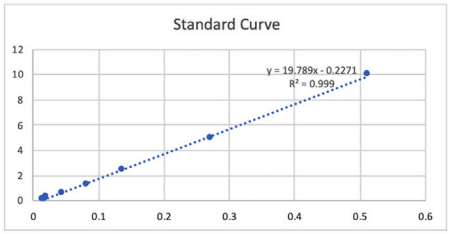

B

	1	2	3	4	5	6	7	8	9	10	11	12
A	0.565	0.581	0.061	0.066	0.063	0.062	0.062	0.066	0.06	0.06	0.061	0.06
B	0.334	0.329	0.056	0.059	0.439	0.531	0.484	0.058	0.063	0.126	0.182	0.13
C	0.188	0.207	0.059	0.063	0.06	0.065	0.075	0.062	0.064	0.077	0.06	0.06
D	0.14	0.145	0.847	0.524	0.536	0.309	0.74	0.911	0.633	0.883	0.061	0.061
E	0.104	0.104	0.059	0.064	0.061	0.067	0.06	0.061	0.061	0.06	0.059	0.06
F	0.08	0.08	0.058	0.058	0.06	0.081	0.062	0.059	0.059	0.06	0.062	0.061
G	0.069	0.082	0.497	0.588	0.695	0.244	0.105	0.099	0.102	0.087	0.364	0.676
H	0.068	0.089	0.296	0.452	0.504	0.135	0.062	0.06	0.059	0.059	0.062	0.061

C

	1	2	3	4	5	6	7	8	9	10	11	12
A	standard(10ng/ml)		NA	NA	PBS#1	PBS#2	PBS#3	6-OHDA#1	6-OHDA#2	6-OHDA#3	NA	NA
B	standard(5ng/ml)		NA	NA	PBS#1	PBS#2	PBS#3	6-OHDA#1	6-OHDA#2	6-OHDA#3	NA	NA
C	standard(2.5ng/ml)		BAT#1	BAT#2	BAT#3	BAT#4	sham#1	sham#2	sham#3	sham#4	NA	NA
D	standard(1.25ng/ml)		BAT#1	BAT#2	BAT#3	BAT#4	sham#1	sham#2	sham#3	sham#4	NA	NA
E	standard(0.625ng/ml)		IL6f/f	IL6f/f	IL6f/f	IL6f/fΔUCP1	IL6f/fΔUCP1	IL6f/fΔUCP1	IL6f/fΔUCP1	IL6f/fΔUCP1	IL6f/f	IL6f/f
F	standard(0.3125ng/ml)		IL6f/f	IL6f/f	IL6f/f	IL6f/fΔUCP1						
G	standard(0.15625ng/ml)		IL6f/f	IL6f/f	IL6f/f	IL6f/fΔUCP1	IL6f/fΔUCP1	IL6f/fΔUCP1	IL6f/fΔUCP1	IL6f/fΔUCP1	IL6f/f	IL6f/f
H	blank		IL6f/f	IL6f/f	IL6f/f	IL6f/fΔUCP1						

Figure S7. Raw Data from ELISA Analysis of IL-6, Related to Figures 1B, 3D, and 3G

(A) The raw data of IL-6 from stressed mice including the standards concentration from Eve Technologies.

(B) The raw OD values from the plate presented in (D).

(C) The layout of samples from the plate presented in (D). Row A, C, E, and F were samples collected before bleeding. Row B, D, G, and H were samples at four hours post bleeding. NA, no samples in the well. Row A and B were related to Figure 3D from mice treated with 6-OHDA 0 and 4 hours post bleeding. Row C and D were from mice with surgical denervation of BAT or sham controls (data not show). Row E, F, G, and H were related to Figure 3G from mice with BAT-specific deletion of *Il6* (*Il6*f/f$^{\Delta UCP1}$) or littermate controls (*Il6*f/f) 0 and 4 hours post bleeding.

(D) The representative plate with color developed with TMB.

(E) The standard curve generated based on the OD value in (A) and concentrations in (B) from column 1 and 2.